Suppl Figure 1

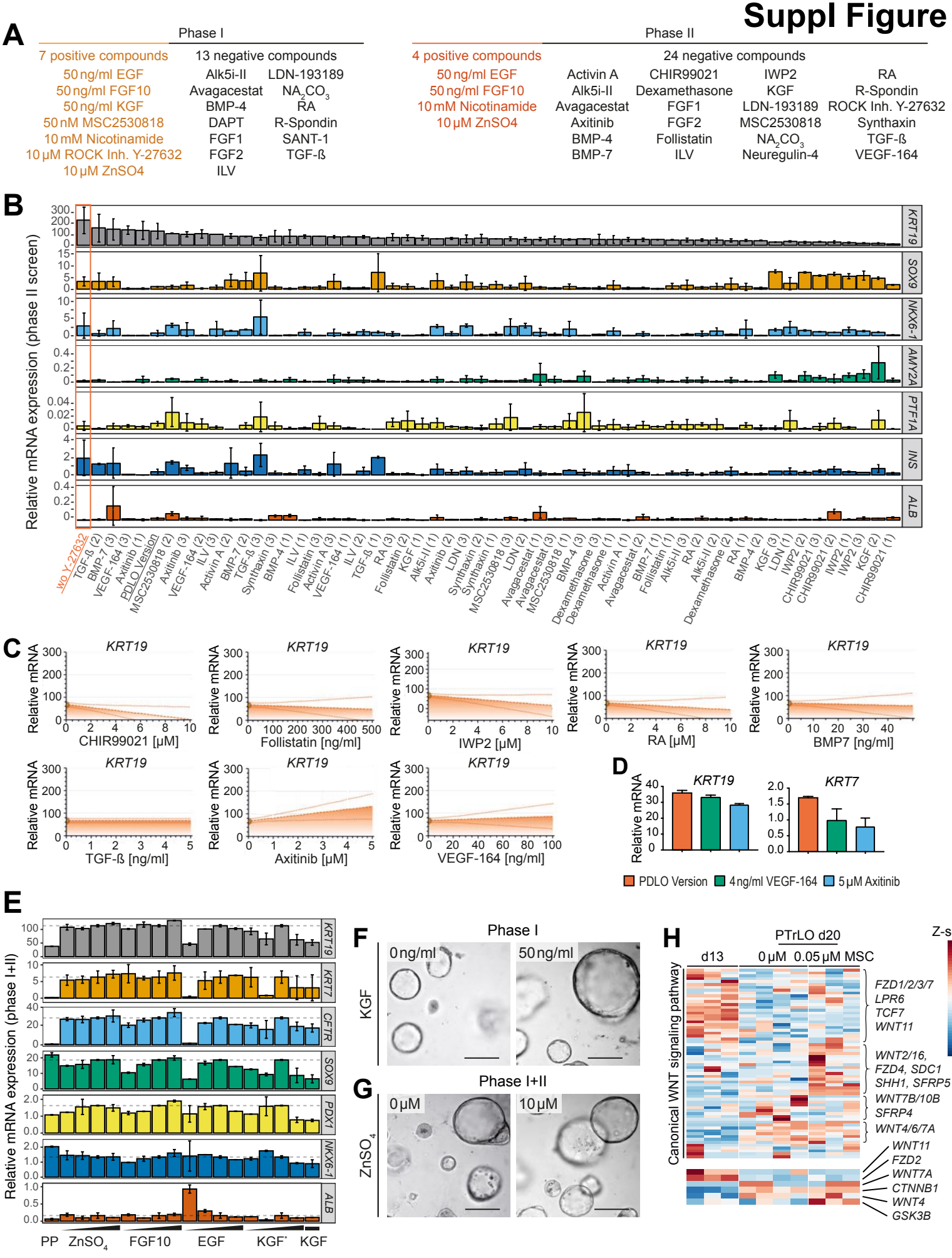

Suppl Figure 2

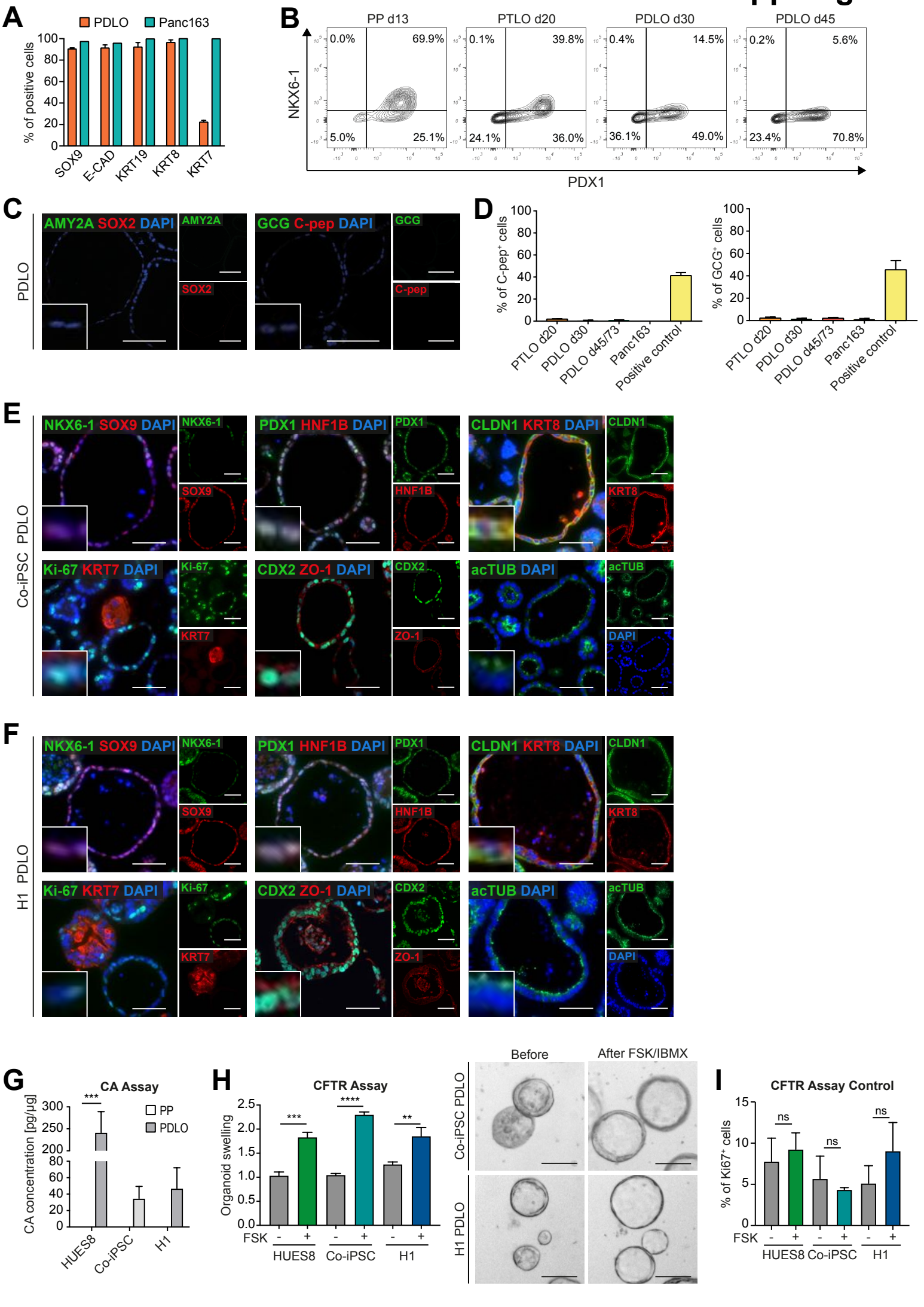

Suppl Figure 3

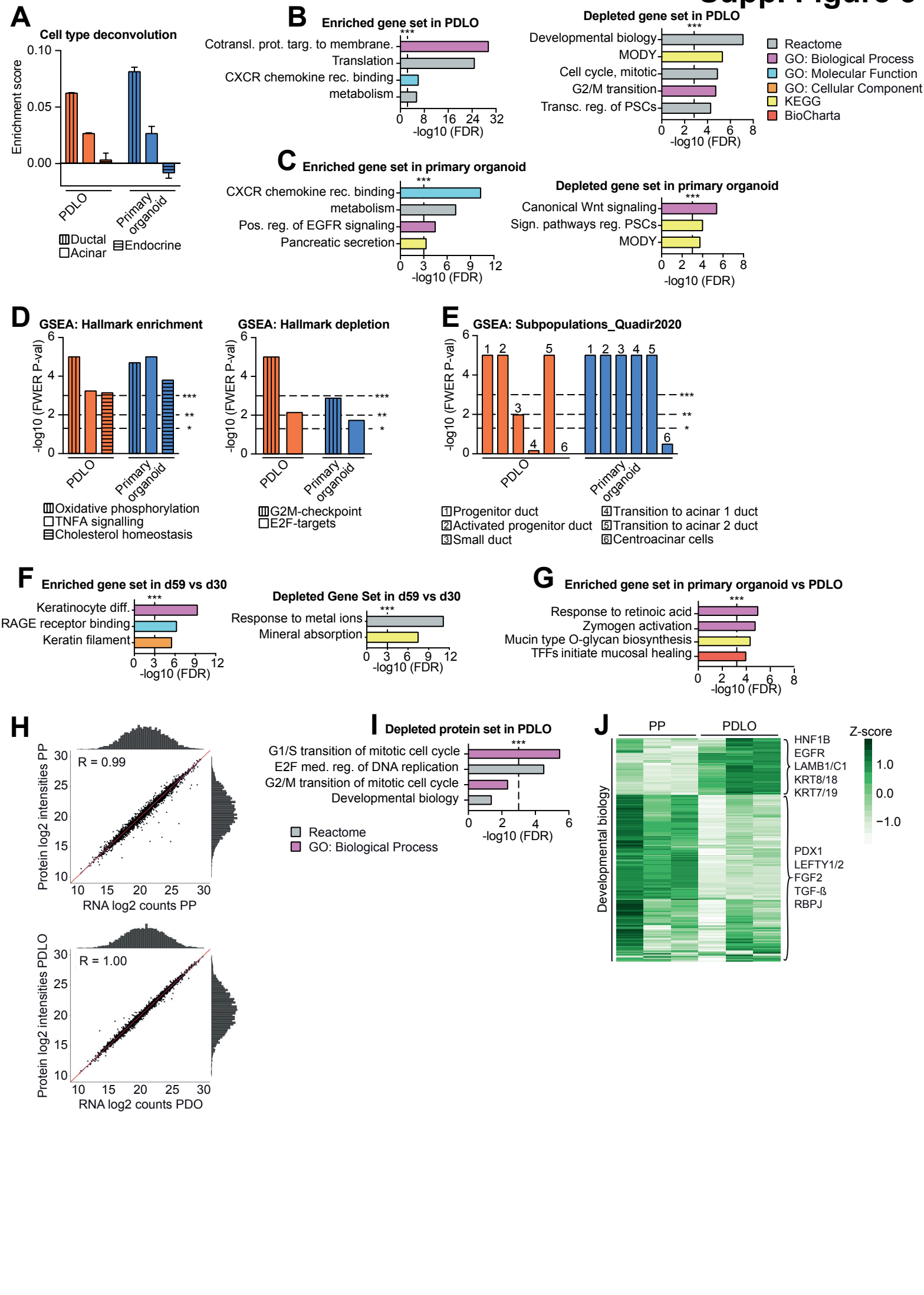

Suppl Figure 4

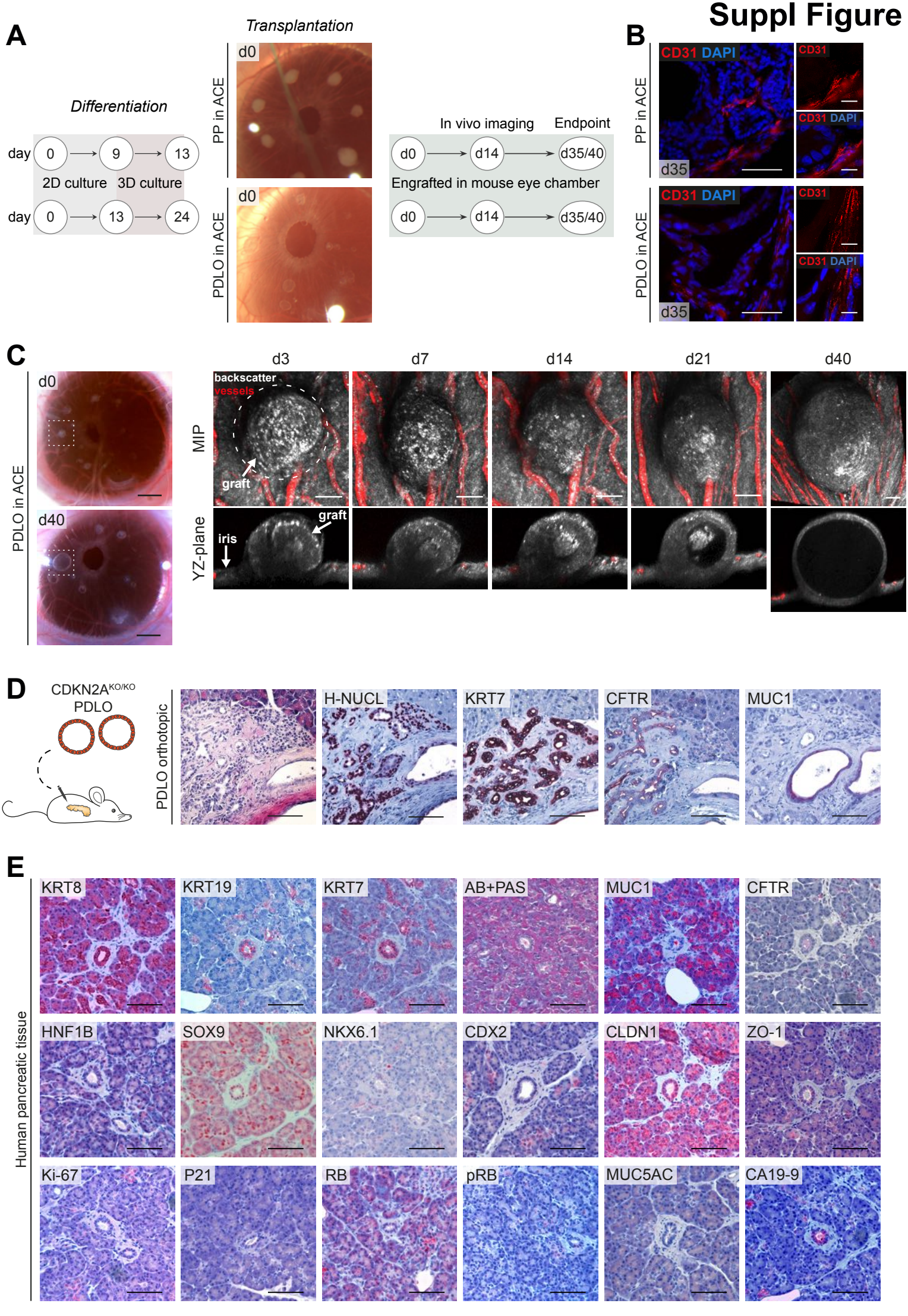

Suppl Figure 5

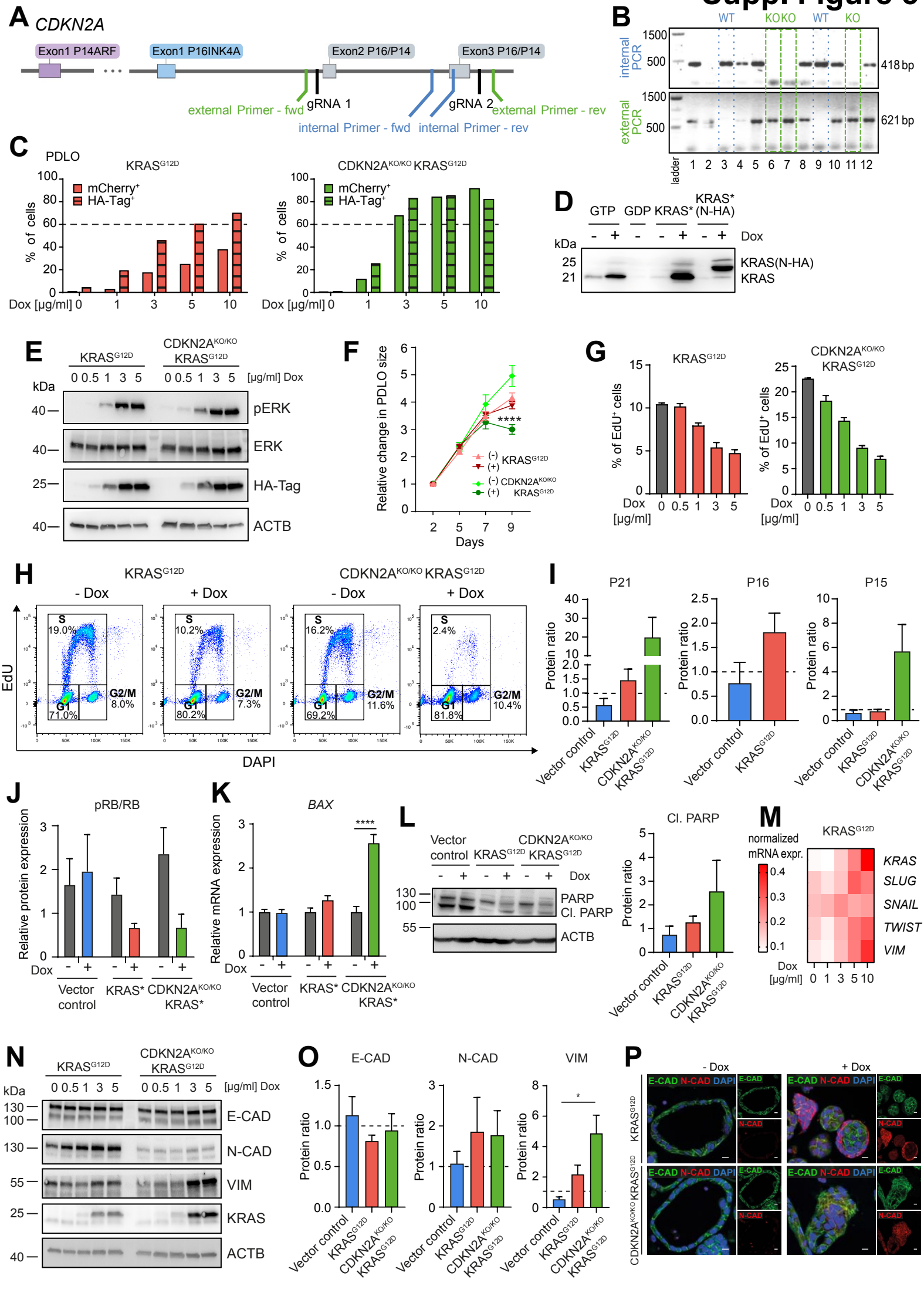

Suppl Figure 6

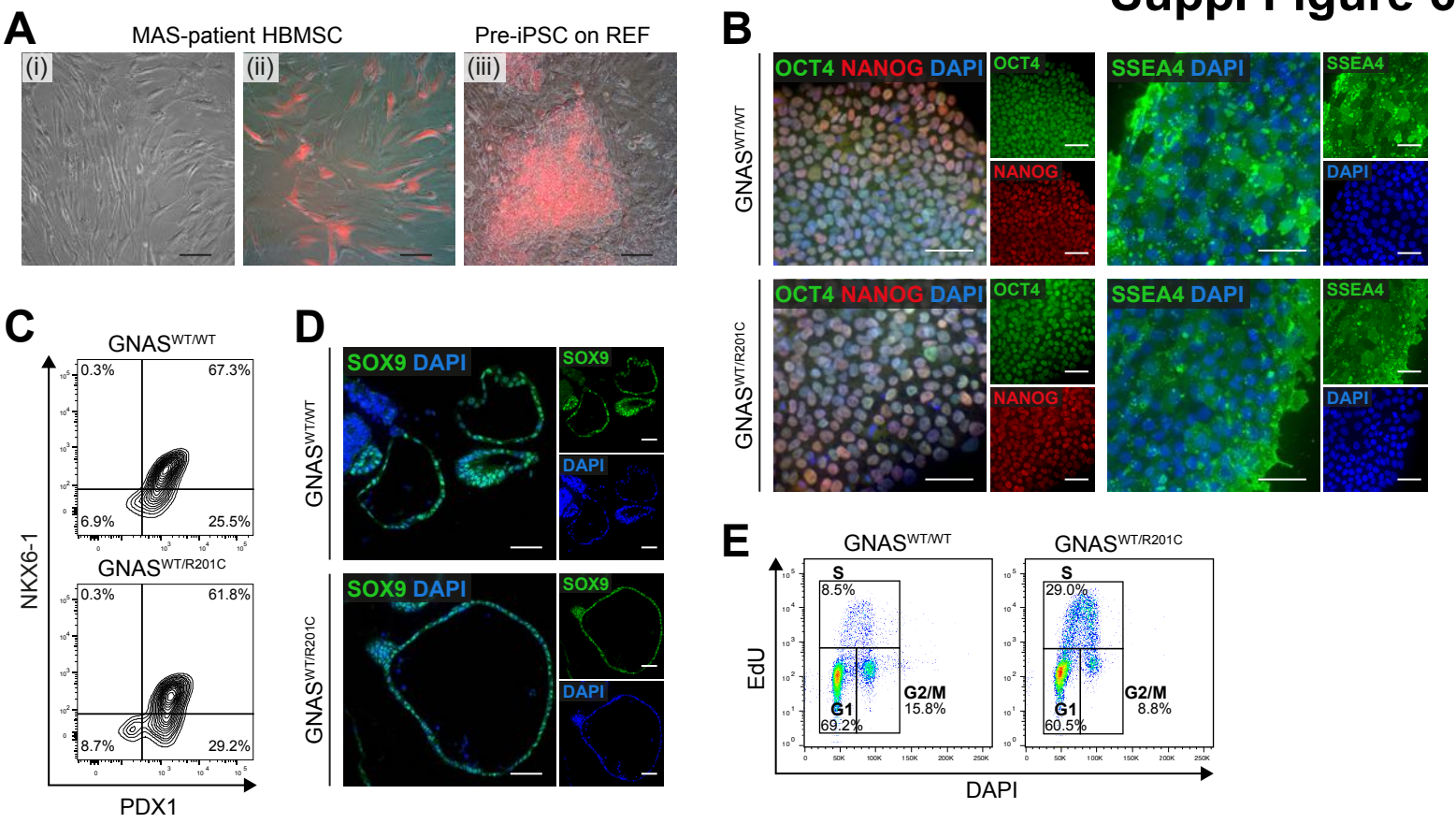

Suppl Figure 7

A

Genotype	Take rate	Reporter expr.	Normal duct	Papillary cystic	Non-cystic lesion	Diff. PDAC	Dediff. PDAC	Atypia/ Dysplasia Low	Atypia/ Dysplasia High	Atypia/ Dysplasia Invasive	MUC5AC	CA19-9	Ki-67
hESC	5/8	-	5/5	0/5	0/5	0/5	0/5	0/5	0/5	0/5	-	-	+
KRAS^{G12D} w/o Dox	2/3	No: 2/2	2/2	0/2	0/2	0/2	0/2	0/2	0/2	0/2	-	-	+
KRAS^{G12D}	7/11	Yes: 4/7	0/4	2/4	1/4	1/4	0/4	1/4	2/4	1/4	++	++	++
		No: 3/7	3/3	0/3	0/3	0/3	0/3	0/3	0/3	0/3	-	-	-
CDKN2A$^{KO/KO}$ KRAS^{G12D} w/o Dox	6/6	No: 6/6	3/6	2/6	1/6	0/6	0/6	3/6	0/6	0/6	+	+	++
CDKN2A$^{KO/KO}$ KRAS^{G12D}	7/7	Yes: 6/7	0/6	0/6	0/6	0/6	6/6	0/6	0/6	6/6	-	-	+++
		No: 1/7	0/1	0/1	1/1	0/1	0/1	1/1	0/1	0/1	-	-	++
GNAS^{R201H} w/o Dox	3/5	No: 3/3	2/3	1/3	0/3	0/3	0/3	0/3	0/3	0/3	-/+	-/+	++
GNAS^{R201H}	9/12	Yes: 8/9	1/8	6/8	1/8	0/8	0/8	6/8	0/8	0/8	+	+	++
		No: 1/9	0/1	0/1	1/1	0/1	0/1	1/1	0/1	0/1	+	-	-

+++ 100%
++ 80%
60%
+ 40%
20%
- 0%

B

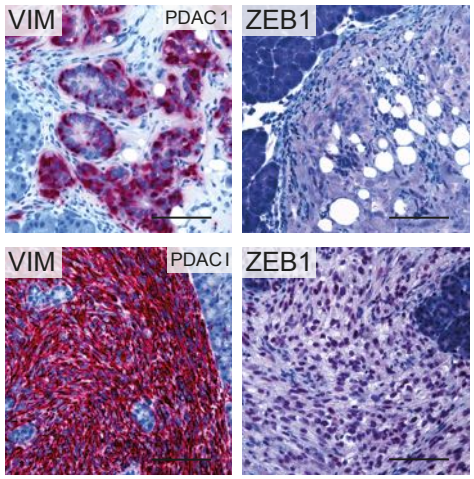

C

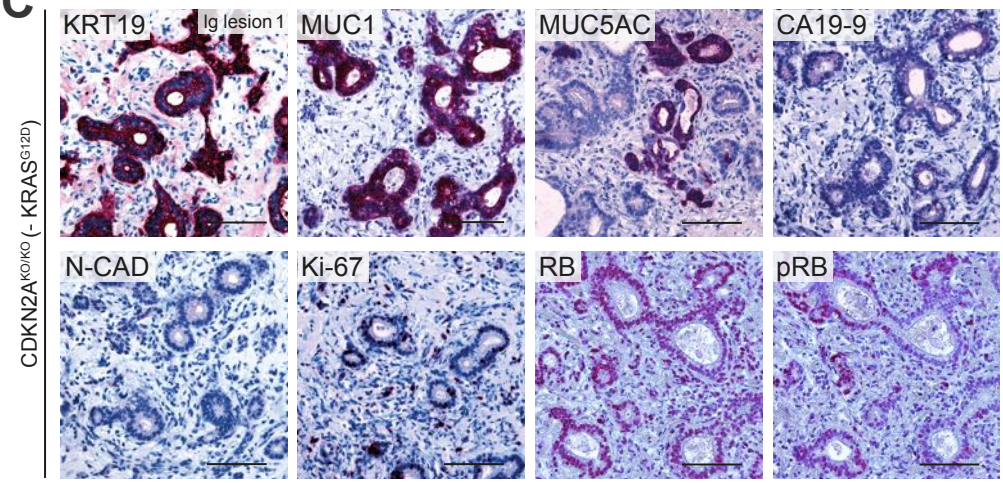

D

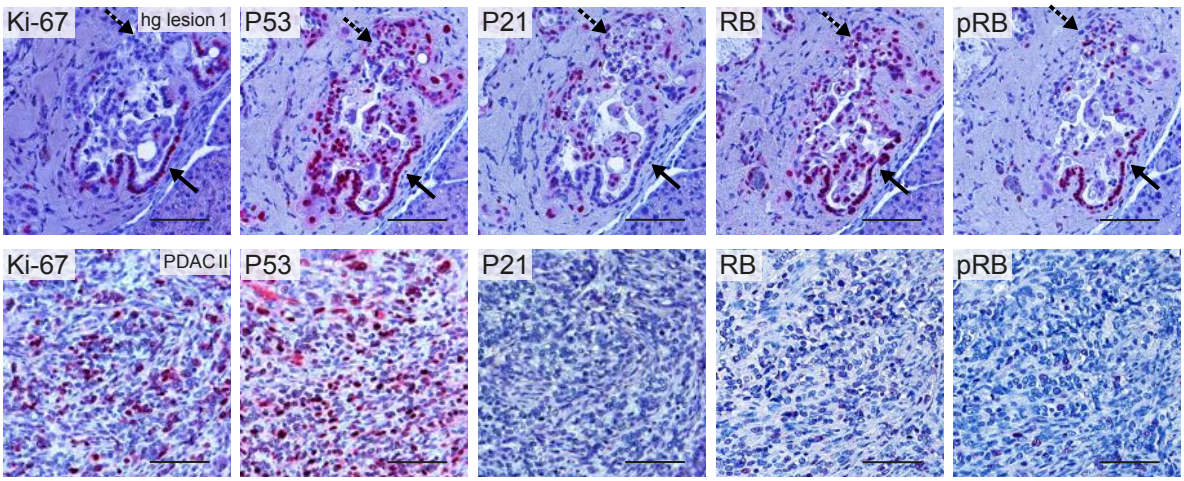

E

Mutations with high annotation impact

CDKN2A$^{KO/KO}$ + KRAS^{G12D} (PDAC II)

TP53_c.280T>C
ETV6_c511delC
FGFR1_c.2142-2A>T
KMT2C_c.2447dupA
MAP3K14_n.763+1dupC
MEN1_c.460A>T
MSH6_c.3367G>T
SETBP1_c.681_682insTCTT

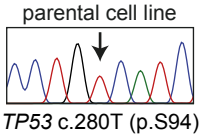

TP53 c.280T (p.S94)

F

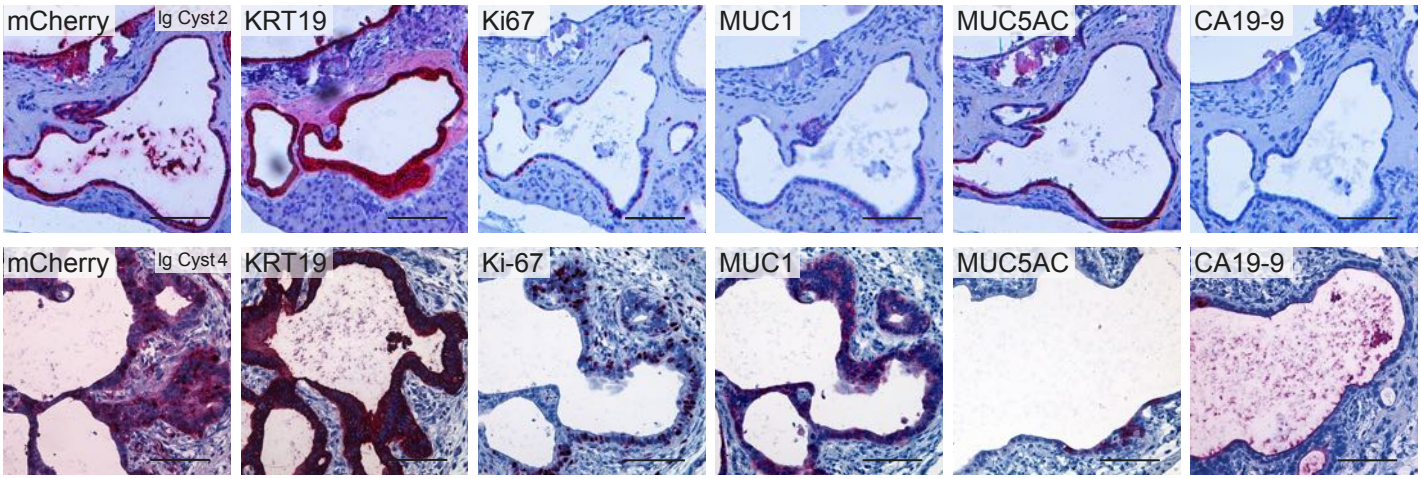

Supplemental Figure Legends

Supplemental Figure 1. Engineering PDLOs from human pluripotent stem cells

(A) Overview of positively and negatively tested compounds during protocol development. **(B,C)** Compound selection in an exemplary screen for phase II. **(B)** Bar graph of tested compounds: Activin A (1: 100 ng/ml, 2: 20 ng/ml, 3: 4 ng/ml), ALK5i-II (1: 5 µM, 2: 1 µM, 3: 0.2 µM), Avagacestat (1: 10 µM, 2: 2 µM, 3: 0.5 µM), Axitinib (1: 5 µM, 2: 1 µM, 3: 0.2 µM), BMP-4 (1: 50 ng/ml, 2: 10 ng/ml, 3: 2 ng/ml), BMP-7 (1: 50 ng/ml, 2: 10 ng/ml, 3: 2 ng/ml), CHIR99021 (1: 10 µM, 2: 2 µM, 3: 0.4 µM), Dexamethasone (1: 2.5 µM, 2: 0.5 µM, 3: 0.1 µM), Follistatin (1: 500 ng/ml, 2: 100 ng/ml, 3: 20 ng/ml), IL-V (1: 1650 nM, 2: 330 nM, 1: 66 nM), IWP2 (1: 10 µM, 2: 2 µM, 3: 0.4 µM), KGF (1: 100 ng/ml, 2: 20 ng/ml, 3: 4 ng/ml), LDN-193189 (1: 1 µM, 2: 0.2 µM, 3: 0.04 µM), MSC2530818 (1: 1 µM, 2: 0.2 µM, 3: 0.05 µM), RA (1: 10 µM, 2: 2 µM, 3: 0.4 µM), Synthaxin (1: 500 ng/ml, 2: 100 ng/ml, 3: 20 ng/ml), TGF-β (1: 5 ng/ml, 2: 1 ng/ml, 3: 0.2 ng/ml), VEGF-164 (1: 100 ng/ml, 2: 20 ng/ml, 3: 4 ng/ml). **(C)** Dynamic profiles of selected compounds that are not used in the current PDLO protocol. Dynamic marker profiles were interpolated from qPCR data using MODDE software. **(D)** Promising compounds like VEGF-164 and Axitinib had been tested in additional experiments and only compounds, which consistently improved morphology and marker expression, were applied in the current protocol. **(E-G)** Positively tested compounds in phase I and phase II complementary to **Fig.1**. **(E)** mRNA expression of selected differentiation markers in PDLOs after treatment with different concentrations of key compounds compared to PPs. Compounds were tested during phase I and II, KGF* only during phase I. Concentration: 0-50 µM $ZnSO_4$, 0-250 ng/ml FGF10, 0-250 ng/ml EGF, 0-250 ng/ml KGF*, 10 ng/ml KGF. Dashed lines indicate expression level of markers reached with the finally chosen concentrations. **(F)** BF images of PDLO cultures at day 30 after KGF titration in phase I. **(G)** BF images of $ZnSO_4$ titration in phase I and II. **(H)** Plotting all identified genes from the GO term “Canonical WNT signaling” (GO:0060070) at PP and PTrLO stage from RNA-seq experiments with or without MSC2530818 treatment in phase I (d13-20). Scale bar: 100 µm. Representative bright field images and dynamic profiles of one experiment performed in technical duplicates (two wells per condition) are displayed as Mean±SD.

Supplemental Figure 2. PDLOs recapitulate cell type-specific features

(A) Quantification of IHC staining in PDLOs and PDAC tumor organoids (Panc163) with exemplary staining of KRT19 and KRT7 (PDLO: n=4, Panc163: n=1, Mean±SEM). **(B)** Exemplary FC plots related to **Fig.2D**. **(C)** IF staining for non-pancreatic marker SOX2, and non-ductal markers amylase (AMY2A), glucagon (GCG), and C-peptide (C-pep) confirming lineage-specificity of the ductal protocol. **(D)** FC analysis of GCG and C-pep. Error bars depict Mean±SEM; d30/45/73: n=3; d20/Panc163/positive control (*in vitro* hPSC-derived polyhormonal endocrine cells): n=2. **(E-I)** Phenotypic and functional characterization of PDLOs generated from a control iPSC line and the ESC line H1 demonstrating transferability of the differentiation protocol to other hPSC lines. **(E,F)** IF staining panel of pancreatic transcription factors and structural proteins in PDLOs recapitulating pancreatic duct-specific cellular features comparable to **Fig.2C,E,F**. **(G,H)** CA and CFTR activity assays indicate ductal functionality of hPSC-derived PDLOs. Right: Representative BF images before and after stimulation in the CFTR assay. **(I)** Ki-67 FC analysis of PDLO cells after performing the CFTR assay with no obvious increase in proliferation in the FSK + IBMX group. All scale bars: 100 µM, insets in the left bottom corner are 4x enlarged. If not stated elsewise, PDLOs represent day 30. **G,H,I**: Error bars depict Mean±SEM; n=3; ordinary one-way Anova followed by Sidak's multiple comparison test.

Supplemental Figure 3. Global transcriptomic and proteomic analyses confirm ductal identity

(A) Cell type deconvolution of PDLOs (d30) and primary ducts calculating similarity scores for the respective samples to the different pancreatic cell types (Enge et al., 2017) based on a recently published algorithm (Frishberg et al., 2019). **(B,C,F,G)** RNA-seq overrepresentation analysis to identify enriched and depleted reference data sets from common databases (KEGG, Reactome, Gene Onotology (GO), BioCharta). **(B,C)** Enriched and depleted gene sets in PDLOs (d30; B) or primary ducts (C) over PPs (d13). **(D, E)** GSEA of PDLOs (d30) and primary ducts against PPs using gene sets from the hallmark database (h.all.v7.0.symbols; D) or gene sets from ductal subpopulations (E) identified in Qadir et al. (2020). PDLOs were enriched for four out of six gene sets. **(F)** Enriched and depleted gene sets in d59 vs d30 of differentiation. **(G)** Gene sets enriched in primary ducts over PDLOs. **(H-J)** Global protein characterization of PDLOs complementing **Fig.3H-N**. **(H)** Pearson Correlation of log2 RNA read counts and log2 protein intensities on PPs (d13) and PDLOs (d59). **(I)** Depleted protein sets in PDLOs over PPs. Overrepresentation analysis was performed against common gene set databases (KEGG, Reactome, GO, BioCharta). **(J)** Exemplary heatmap of the in (**I**) depleted protein data set "Developmental Biology".

Supplemental Figure 4. Development of human duct-like tissue after xenotransplantation of PDLOs

(A) Experimental setup and timeline of PP or PDLO transplantation into the anterior chamber of the mouse eye (ACE). Images show grafts right after injection onto the iris. **(B)** CD31-positive endothelial cells surrounding grafts from PPs or PDLOs five weeks post transplantation. Scale bar: 50 µm for overview, 10 µm for higher magnification. **(C)** Longitudinal live imaging *in vivo* over five weeks post transplantation. Left: Overview of the eye with tracked PDLO (dashed rectangle) at the beginning (d0) and end (d40) of the experiment. Right: Images show maximum intensity projections (MIP) of backscatter signal of a single PDLO engraftment (dashed circle) and blood vessels (red) in the ACE visualized by i.v. injection of FITC-Dextran. Cells with high backscatter signal are highly granulated cells. Bottom right: YZ-plane showing development of a large cell-free lumen within the engrafted PDLO. **(D)** Orthotopic transplantation of CDKN2A$^{KO/KO}$ hESC-derived PDLOs. Formation of CFTR- and MUC1-positive subpopulations in such PDLO grafts (H-NUCL, human nucleoli). **(E)** IF staining of human untransformed ducts from a pancreatic biopsy. Scale bar: 500 µm for overview. All scale bars: 100 µM, if not stated elsewise.

Supplemental Figure 5. KRAS^{G12D} expression induces lumen-filling and EMT in PDLOs

(A,B) *CDKN2A* gene KO in hESCs by CRISPR/Cas9 gene editing. **(A)** Strategy for creating a large deletion in the *CDKN2A* locus using CRISPR/Cas9. The schema displays the positions of guide RNAs, as well as external and internal primers used for KO validation by PCR. **(B)** Cells were clonally expanded and screened by PCR with an internal and external primer pair detecting the WT and mutated target region, respectively. The external PCR only amplifies a product if the desired deletion has occurred. Successful identification of targeted hESC clones with heterozygous or homozygous loss of *CDKN2A*. **(C-P)** Further charaterization of PDLOs differentiated from vector control, KRAS^{G12D} and CDKN2A$^{KO/KO}$ KRAS^{G12D} transgenic lines. **(C)** Titration of Dox concentration to activate the expression of HA-tagged KRAS^{G12D} transgene. FC analysis of mCherry and HA-Tag expression after 9 days showed robust transgene induction in PDLOs with 5 µg/ml Dox (n=1). **(D)** Functionality of the cloned KRAS^{G12D} construct with and without HA-tag was verified by active-KRAS pull-down assay and subsequent Western Blot. GTP was added in additional controls to activate endogenous KRAS. KRAS*: KRAS^{G12D}. **(E)** Western Blot analysis confirmed the dose-dependent increase in transgene expression as well as phosphorylation of the KRAS downstream target pERK. **(F)** PDLO size measured by image-based area quantification after 2, 5, 7, and 9 days with and without Dox treatment of PDLOs. Size change is shown relative to d2 (n=3). **(G)** Continuous decrease of replicating cells in PLDOs treated with increasing doses of Dox, assessed by EdU-based FC analysis (n=1, in technical duplicates). **(H)** Representative plots of FC analysis to determine cell cycle stages and proliferation of PDLOs after EdU incorporation. **(I,J)** Quantification of western blot analyses representatively shown in **Fig.5G**. **(I)** Protein expression was normalized to a housekeeping protein and relative expression to untreated samples is displayed. P21 (n≥4); P16 (n≥2); P15 (n≥3). **(J)** pRB relative protein expression is shown after normalization to total RB (n=4). **(K)** Pro-apoptotic *BAX* was upregulated on mRNA level in CDKN2A$^{KO/KO}$ KRAS^{G12D} PDLOs (n=3). **(L)** Western Blot detection of apoptosis-associated cleaved PARP and respective quantification (n≥2). **(M)** Heatmap illustrating mRNA expression of EMT-associated genes in a KRAS^{G12D} (Dox) titration qPCR experiment (n=1). **(N)** Western Blot analysis of KRAS and EMT-associated marker after Dox titration inCDKN2A$^{KO/KO}$ and CDKN2A$^{WT/WT}$ KRAS^{G12D} PDLOs (n=1). **(O)** Quantification of western blot analyses representatively shown in **Fig.5K**. E-CAD, N-CAD, VIM (n≥4). **(P)** IF staining of PDLOs for epithelial and mesenchymal (N-CAD, N-Cadherin) markers. Scale bar: 10 µm. For all subfigures: Error bars depict Mean±SEM. Only significant comparisons are depicted. F,J,K: Ordinary two-way Anova with Sidak's multiple comparison test. I,L,O: Ordinary one-way Anova with Tukey's multiple comparison test.

Supplemental Figure 6. McCune-Albright syndrome-derived and GNAS^{R201H} overexpressing PDLOs form large cysts (A) Reprogramming of a mixed culture of GNAS$^{WT/WT}$ and GNAS$^{WT/R201C}$ cells from an MAS patient. (i) BF images of MAS patient-derived human bone marrow stromal cells (HBMSCs), (ii) overlay with fluorescence signal from hOKSM-dTomato reprogramming virus, and (iii) pre-iPSC colony formed on REF feeder layer. **(B)** IF staining of MAS-iPSC colonies for pluripotency markers (OCT4, Octamer-binding transcription factor 4; NANOG, Homeobox protein NANOG; SSEA4; Stage-specific embryonic antigen-4). **(C)** Representative FC plots demonstrating efficient differentiation of both GNAS$^{WT/WT}$ and GNAS$^{WT/R201C}$ iPSCs to PDX1^{+}/NKX6-1^{+} PPs (d13). **(D)** IF staining of PDLOs revealing homogeneous SOX9 expression irrespective of their GNAS genotype. **(E)** Representative FC plots acquired to analyze cell proliferation of PDLOs based on EdU incorporation. **(F)** FC-based quantification of mCherry reporter expression indicative for robust transgene induction after Dox treatment in hESCs (1-2 days) and respective PDLOs (9 days) harboring a *piggyBac* vector control or GNAS^{R201H} expression cassette (n=2, except GNAS^{R201H} hESC: n=3). **(G)** PDLO size measured by image-based area quantification after 2, 5, 7, and 9 days with and without Dox treatment of PDLOs. Size change is shown relative to d2 (n=3). **(H)** Quantification of cAMP assay performed with GNAS^{R201H} hESCs or PDLOs displaying upregulation of cAMP levels upon Dox-induced oncogene expression. FSK was added as positive control to stimulate cAMP production (n=1 in technical triplicates). All scale bars: 50 µM. Error bars depict Mean±SEM; G: ordinary two-way Anova with Sidak's multiple comparison test.

Supplemental Figure 7. Mutation-dependent PDAC- or IPMN-like tumor formation from PDLO grafts

(A) Summary of engraftment types resulting from orthotopically transplanted PDLOs after eight weeks. Cellular atypia and tissue dysplasia were carefully examined to allow grading into normal duct, low- or high-grade lesion, and invasive cancer. Grafts were classified according to the highest grade of lesion found within one graft. Marker (MUC5AC, CA19-9, Ki-67) expression was averaged over individual grafts of each genotype (–, completely or nearly absent; +, weak expression; ++, moderate expression; +++, strong expression). **(B)** IHC staining confirming a well-differentiated PDAC phenotype after $KRAS^{G12D}$ induction alone and an almost completely undifferentiated PDAC phenotype after $KRAS^{G12D}$ induction in $CDKN2A^{KO/KO}$ PDLO grafts (ZEB1, Zinc finger E-box binding homeobox 1). **(C)** Increased tumor marker expression (MUC5AC) in well-differentiated $CDKN2A^{KO/KO}$ PDLO-derived grafts without KRAS induction. **(D)** Staining of cell cycle-associated proteins in respective tumor sites depicted in **Fig.7B** (hg lesion 1, PDAC II). Very few P21 positive cells could be detected in the tumor derived from $CDKN2A^{KO/KO}$ $KRAS^{G12D}$ PDLO grafts. As complementary mechanism to hyperphosphorylation of RB indicated for PDAC I in **Fig.7E**, RB protein appeared downregulated in $CDKN2A^{KO/KO}$ $KRAS^{G12D}$-derived PDAC II. Arrows in hg lesion 1 highlight a proliferative region, while dashed arrows depict a region with mainly intact P53/P21 and RB/pRB checkpoint control resulting in very low proliferation. **(E)** Panel-sequencing of $CDKN2A^{KO/KO}$ $KRAS^{G12D}$ PDAC II. All mutations, which were predicted to be likely pathogenic are shown. Of note, we detected an as pathogenic described $P53^{S94P}$ missense mutation with 25% allele frequency. **(F)** IHC staining of two $GNAS^{R201H}$ grafts supporting IPMN-like tumor formation in $GNAS^{R201H}$ grafts and revealing heterogeneity in MUC5AC and CA19-9 expression between different cysts. Overview HE staining of these grafts are shown in **Fig.7H**. Scale bar: 100 µM, except for HE staining. Scale bar in HE overviews: 500 µm; in insets: 50 µm.

Supplemental Table 1. Copy number variations identified in PDAC1, PDACI, and III using lcWGS
Please refer to separate Excel sheet.

Supplemental Table 2. Point mutations identified in PDACII using a targeted sequencing approach
Please refer to separate Excel sheet.

Supplemental Table 3. Primers used in this study for cloning of plasmids

Primer	Sequence
attB1-SpeI-HindIII-(N-HA)-KRAS^{G12D}-fwd	aaaaagcaggcttcactagtgtctttcataagcttatgtatccatatgatgtgcccgact
attB2-KRAS^{G12D}-rev	agaaagctgggtgtgacacacattccacagggt
attB1-SpeI-HindIII-GNAS(EE)^{R201H}-fwd_new	aaaaagcaggcttcactagtgtctttcataagcttatgggctgcctcgggaac
attB2-GNAS^{R201H}-rev_new	agaaagctgggtgttagagcagctcgtactgacg
attB1-Luc2-for	aaaaagcaggcttcgccaccatggaagatgccaaa
attB2-Luc2-rev	agaaagctgggtgttacacggcgatcttgccgcccttc
PB-seq-fwd	agctcgtttagtgaaccgtcagatc
PB-seq-rev	gtacaagaaagctgggt
GNAS_AS189-fwd	aatatatgccgaccgagcagg
Luc2_AS215-fwd	cgcttgtgtccgattcagtc

Supplemental Table 4. Composition of solutions for ion secretion and uptake experiments

	Standard HEPES	**Na-Free HCO_3^-**	**Standard HCO_3^-**	**NH_4Cl^- HCO_3^-**
NaCl	130	-	115	95
KCl	5	5	5	5
$MgCl_2$	1	1	1	1
$CaCl_2$	1	1	1	1
Hepes	10	-	-	-
Glucose	10	10	10	10
$NaHCO_3^-$	-	-	25	25
EGTA	-	-	-	-
NH_4Cl	-	-	-	20
NMDG	-	115	-	-
Choline HCO_3^-	-	25	-	-
Atropine	-	0.01	-	-

Supplemental Table 5. Self-designed or commercially available qPCR primers used in this study

Gene	Forward primer sequence (fwd)	Reverse primer sequence (rev)	QuantiTect Cat#
ALB	-	-	QT00063693*
AMY2A	-	-	QT01680595*
BAX	tggagctgcagaggatgattg	gaagttgccgtcagaaaacatg	
CFTR	-	-	QT00070007*

FN1	-	-	QT00038024*
GCG	-	-	QT00091756*
HMBS	-	-	QT00494130*
INS	-	-	QT01531040*
KRAS	-	-	QT00083622*
KRT19	ctacagccactactacacgac	cagagcctgttccgtctcaaa	
KRT7	ggagccgtgaatatctctgtga	tgcggtccggatggaataag	
N-CAD	-	-	QT00063196*
NKX6-1			QT00092379*
P21	gcgccatgtcagaaccgcct	gcaggcttcctgtgggcgga	
PDX1	-	-	QT00201859*
PTF1A	-	-	QT01033396*
RELA	atagaagagcagcgtgggga	ttgggggcacgattgtcaaa	
SLUG	cagtgattatttccccgtatc	ccccaaagatgaggagtatc	
SNAIL	gctccttcgtccttctcctc	tgacatctgagtgggtctgg	
SOX4	-	-	QT00220605*
SOX9	-	-	QT00001498*
TWIST1	ctagatgtcattgtttccagag	ccctgtttctttgaatttgg	
VIM	gacaatgcgtctctggcacgtctt	tcctccgcctcctgcaggttctt	
ZEB1	aaagatgatgaatgcgagtc	tccattttcatcatgaccac	

*Primer sequences for commercial Qiagen primers are not available.

Supplemental Table 6. IHC/IF conditions for antibodies used in this study

Embedding	Antibody	Species	Company	Catalogue no.	Condition	Dilution
paraffin	AcTUB	rabbit	Abcam	ab179484	MW Citrat	1000
paraffin	AMY2A	rabbit	Sigma	A8273-1VL	MW Citrat	300
paraffin	C-pep	rabbit	Cell Signaling	4593	MW Citrat	100
paraffin	CA19-9	mouse	Thermo	116-NS-19-9	MW Citrat	500
paraffin	CDX2	rabbit	Cell Marque - RabMab	MU392-UC	MW Citrat	500
paraffin	CFTR	mouse	R&D	MAB1660	ST Tris	200
paraffin	CLDN1	rabbit	Abcam	ab15098	ST Tris	100
paraffin	E-CAD	mouse	Dako	M3612	PC Citrat	100
paraffin	E-CAD	mouse	BD Bioscience	610182	MW Citrat	1000
paraffin	GCG	mouse	Sigma	G2654	MW Citrat	500
paraffin	GFP	rabbit	Thermo	A6455	No AGR	1500
paraffin	H-NUCL	mouse	Abcam	ab190710	MW Citrat	200
paraffin	HA-Tag	rabbit	Cell Signaling	3724	MW Citrat	500
paraffin	HNF1B	mouse	Abcam	ab236759	MW Citrat	100
paraffin	Ki-67	rabbit	Thermo	MA5-14520	MW Citrat	100
paraffin	Ki-67	mouse	Dako	M7240	MW Citrat	200
paraffin	KRT19 (IF)	mouse	Dako	M0888	MW Citrat	100
paraffin	KRT19 (IHC)	mouse	Dako	M0888	Pronase	100
paraffin	KRT7 (IF)	mouse	Dako	M7018	MW Citrat	200

paraffin	KRT7 (IHC)	mouse	Dako	M7018	Pronase	200
paraffin	KRT8	mouse	BD Bioscience	345779	ST Tris	100
paraffin	mCherry	rabbit	Abcam	ab167453	No AGR	500
paraffin	MUC1	mouse	Santa Cruz	sc-7313	MW Citrat	100
paraffin	MUC5AC	mouse	Santa Cruz	sc-33667	MW Citrat	50
paraffin	N-CAD	rabbit	Cell Signaling	13116	MW Citrat or ST Tris	100
paraffin	NKX6-1	mouse	DSHB Hybridoma	F55A12 (concentrate)	MW Citrat	150
paraffin	P21	rabbit	Abcam	ab109520	MW Citrat	300
paraffin	P53	mouse	Santa Cruz	sc-47698	MW Citrat	100
paraffin	PDX1	goat	R&D	AF2419	MW Citrat	500
paraffin	PKC	rabbit	Abcam	ab59364	MW Citrat	200
paraffin	pRB	rabbit	Cell Signaling	8516	ST Citrat	200
paraffin	RB	mouse	Cell Signaling	9309	ST Citrat	400
paraffin	SOX9	rabbit	Millipore	AB5535	MW Citrat	500
paraffin	Turbo GFP	Rabbit	Thermo	PA5-22688	ST Tris	250
paraffin	VIM	rabbit	Cell Signaling	5741S	MW Citrat	500
paraffin	Zeb1	rabbit	Santa Cruz	sc-25388	PC Citrat	300
paraffin	ZO1	mouse	Thermo	33-9100	MW Citrat	500
cryo	C-pep	rabbit	Cell Signaling	#4593	No AGR	100
cryo	CD31	rat	BD Bioscience	557355	No AGR	100
cryo	CTRC	mouse	Millipore	MAB1476	No AGR	1200
cryo	GCG	mouse	Sigma	G2654	No AGR	500
cryo	E-CAD	rabbit	Cell Signaling	3195	No AGR	200
cryo	KRT7	mouse	Dako	M7018	No AGR	200
cryo	KRT8	mouse	BD Bioscience	345779	No AGR	100
cryo	KRT19	mouse	Dako	M0888	No AGR	100
cyro	CFTR	rabbit	Alomone	ACL-006	HB 94°C Citrat/Tween	200
cyro	Occludin	mouse	Thermo	33-1500	HB 94°C Citrat/Tween	200

*MW, microwave; No AGR, no antigen retrieval; PC, pressure cooker; ST, steamer; HB, heating block;

Supplemental Table 7. Reference gene sets used within this study
Please refer to separate Excel sheet.

Supplemental Item Legends

Supplemental Table 1. Copy number variations identified in PDAC 1, PDAC I, and III using lcWGS

Related to **Fig.7F** (Results)

CNV with a log_2ratio ≥ I0.75I are depicted.

Supplemental Table 2. Point mutations identified in PDAC II using a targeted sequencing approach

Related to **Suppl.Fig.7E** (Results)

Point mutations identified in a comprehensive cancer panel (Qiagen). Variants marked in red are not reliable, as clarified in the "tag-defs" spreadsheet.

Supplemental Table 3. Primers used in this study for cloning of plasmids

Related to "*All-in-One piggyBac*-system and Nucleofection" (Methods)

Supplemental Table 4. Composition of solutions for ion secretion and uptake experiments

Related to "*pH measurements via fluorescence microscopy*" (Methods)

Supplemental Table 5. Self-designed or commercially available qPCR primers used in this study

Related to "RNA isolation, reverse transcription and qPCR" (Methods)

*Primer sequences for commercial Qiagen primers are not available.

Supplemental Table 6. IHC/IF conditions for antibodies used in this study

Related to "IF and IHC staining" (Methods)

*MW, microwave; ST, steamer; PC, pressure cooker

Supplemental Table 7. Reference gene sets used within this study

Related to "Gene set enrichment analysis" (Methods)

Video S1. Live-cell imaging of CDKN2A$^{KO/KO}$ KRAS^{G12D} PDLOs w/o Dox stimulation

Related to **Fig.5.M**

Time-lapse video of PDLO culture monitored every 3 h over 4 days. The frame rate was 5 frames per second (fps).

Video S2. Live-cell imaging of CDKN2A$^{KO/KO}$ KRAS^{G12D} PDLOs + Dox stimulation

Related to **Fig.5.M**

Time-lapse video of PDLO culture monitored every 3 h over 4 days. The frame rate was 5 frames per second (fps) and the red mCherry fluorescence signal indicates KRAS^{G12D} expression.

Supplemental Item Legends

Supplemental Table 1. Copy number variations identified in PDAC 1, PDAC I, and III using lcWGS

Related to **Fig.7F** (Results)

CNV with a log_2ratio ≥ I0.75I are depicted.

Supplemental Table 2. Point mutations identified in PDAC II using a targeted sequencing approach

Related to **Suppl.Fig.7E** (Results)

Point mutations identified in a comprehensive cancer panel (Qiagen). Variants marked in red are not reliable, as clarified in the "tag-defs" spreadsheet.

Supplemental Table 3. Primers used in this study for cloning of plasmids

Related to "*All-in-One piggyBac*-system and Nucleofection" (Methods)

Supplemental Table 4. Composition of solutions for ion secretion and uptake experiments

Related to "*pH measurements via fluorescence microscopy*" (Methods)

Supplemental Table 5. Self-designed or commercially available qPCR primers used in this study

Related to "RNA isolation, reverse transcription and qPCR" (Methods)

*Primer sequences for commercial Qiagen primers are not available.

Supplemental Table 6. IHC/IF conditions for antibodies used in this study

Related to "IF and IHC staining" (Methods)

*MW, microwave; ST, steamer; PC, pressure cooker

Supplemental Table 7. Reference gene sets used within this study

Related to "Gene set enrichment analysis" (Methods)

Video S1. Live-cell imaging of CDKN2A$^{KO/KO}$ KRAS^{G12D} PDLOs w/o Dox stimulation

Related to **Fig.5.M**

Time-lapse video of PDLO culture monitored every 3 h over 4 days. The frame rate was 5 frames per second (fps).

Video S2. Live-cell imaging of CDKN2A$^{KO/KO}$ KRAS^{G12D} PDLOs + Dox stimulation

Related to **Fig.5.M**

Time-lapse video of PDLO culture monitored every 3 h over 4 days. The frame rate was 5 frames per second (fps) and the red mCherry fluorescence signal indicates KRAS^{G12D} expression.

Literature:

Afelik, S., and Jensen, J. (2013). Notch signaling in the pancreas: patterning and cell fate specification. Wiley interdisciplinary reviews Developmental biology *2*, 531-544.

Afelik, S., Qu, X., Hasrouni, E., Bukys, M.A., Deering, T., Nieuwoudt, S., Rogers, W., Macdonald, R.J., and Jensen, J. (2012). Notch-mediated patterning and cell fate allocation of pancreatic progenitor cells. Development *139*, 1744-1753.

Aiello, N.M., Brabletz, T., Kang, Y., Nieto, M.A., Weinberg, R.A., and Stanger, B.Z. (2017). Upholding a role for EMT in pancreatic cancer metastasis. Nature *547*, E7-E8.

Aiello, N.M., Maddipati, R., Norgard, R.J., Balli, D., Li, J., Yuan, S., Yamazoe, T., Black, T., Sahmoud, A., Furth, E.E.*, et al.* (2018). EMT Subtype Influences Epithelial Plasticity and Mode of Cell Migration. Dev Cell *45*, 681-695.e684.

Aiello, N.M., Rhim, A.D., and Stanger, B.Z. (2016). Orthotopic Injection of Pancreatic Cancer Cells. Cold Spring Harb Protoc *2016*, pdb.prot078360.

Ansieau, S., Bastid, J., Doreau, A., Morel, A.P., Bouchet, B.P., Thomas, C., Fauvet, F., Puisieux, I., Doglioni, C., Piccinin, S.*, et al.* (2008). Induction of EMT by twist proteins as a collateral effect of tumor-promoting inactivation of premature senescence. Cancer Cell *14*, 79-89.

Baron, M., Veres, A., Wolock, S.L., Faust, A.L., Gaujoux, R., Vetere, A., Ryu, J.H., Wagner, B.K., Shen-Orr, S.S., Klein, A.M.*, et al.* (2016). A Single-Cell Transcriptomic Map of the Human and Mouse Pancreas Reveals Inter- and Intra-cell Population Structure. Cell Syst *3*, 346-360 e344.

Bartek, J., Bartkova, J., and Lukas, J. (2007). DNA damage signalling guards against activated oncogenes and tumour progression. Oncogene *26*, 7773-7779.

Benjamini, Y., and Hochberg, Y. (1995). Controlling the false discovery rate: a practical and powerful approach to multiple testing. Journal of the Royal statistical society: series B (Methodological) *57*, 289-300.

Bianco, P., Kuznetsov, S.A., Riminucci, M., Fisher, L.W., Spiegel, A.M., and Robey, P.G. (1998). Reproduction of human fibrous dysplasia of bone in immunocompromised mice by transplanted mosaics of normal and Gsalpha-mutated skeletal progenitor cells. The Journal of clinical investigation *101*, 1737-1744.

Biederstädt, A., Hassan, Z., Schneeweis, C., Schick, M., Schneider, L., Muckenhuber, A., Hong, Y., Siegers, G., Nilsson, L., and Wirth, M. (2020). SUMO pathway inhibition targets an aggressive pancreatic cancer subtype. Gut.

Blondel, V.D., Guillaume, J.-L., Lambiotte, R., and Lefebvre, E. (2008). Fast unfolding of communities in large networks. Journal of statistical mechanics: theory and experiment *2008*, P10008.

Boj, S.F., Hwang, C.I., Baker, L.A., Chio, II, Engle, D.D., Corbo, V., Jager, M., Ponz-Sarvise, M., Tiriac, H., Spector, M.S.*, et al.* (2015). Organoid models of human and mouse ductal pancreatic cancer. Cell *160*, 324-338.

Boj, S.F., Hwang, C.I., Baker, L.A., Engle, D.D., Tuveson, D.A., and Clevers, H. (2016). Model organoids provide new research opportunities for ductal pancreatic cancer. Molecular & cellular oncology *3*, e1014757.

Bolger, A.M., Lohse, M., and Usadel, B. (2014). Trimmomatic: a flexible trimmer for Illumina sequence data. Bioinformatics *30*, 2114-2120.

Brion, L.P., Schwartz, J.H., Zavilowitz, B.J., and Schwartz, G.J. (1988). Micro-method for the measurement of carbonic anhydrase activity in cellular homogenates. Analytical biochemistry *175*, 289-297.

Burghardt, B., Elkaer, M.L., Kwon, T.H., Racz, G.Z., Varga, G., Steward, M.C., and Nielsen, S. (2003). Distribution of aquaporin water channels AQP1 and AQP5 in the ductal system of the human pancreas. Gut *52*, 1008-1016.

Caldwell, M.E., DeNicola, G.M., Martins, C.P., Jacobetz, M.A., Maitra, A., Hruban, R.H., and Tuveson, D.A. (2012). Cellular features of senescence during the evolution of human and murine ductal pancreatic cancer. Oncogene *31*, 1599-1608.

Campisi, J. (2013). Aging, cellular senescence, and cancer. Annual review of physiology *75*, 685-705.

Chan-Seng-Yue, M., Kim, J.C., Wilson, G.W., Ng, K., Figueroa, E.F., O'Kane, G.M., Connor, A.A., Denroche, R.E., Grant, R.C., McLeod, J.*, et al.* (2020). Transcription phenotypes of pancreatic cancer are driven by genomic events during tumor evolution. Nat Genet *52*, 231-240.

Chen, Z., Trotman, L.C., Shaffer, D., Lin, H.K., Dotan, Z.A., Niki, M., Koutcher, J.A., Scher, H.I., Ludwig, T., Gerald, W.*, et al.* (2005). Crucial role of p53-dependent cellular senescence in suppression of Pten-deficient tumorigenesis. Nature *436*, 725-730.

Chmelova, H., Cohrs, C.M., Chouinard, J.A., Petzold, C., Kuhn, M., Chen, C., Roeder, I., Kretschmer, K., and Speier, S. (2015). Distinct roles of β-cell mass and function during type 1 diabetes onset and remission. Diabetes *64*, 2148-2160.

Cho, C.H., Hannan, N.R., Docherty, F.M., Docherty, H.M., Joao Lima, M., Trotter, M.W., Docherty, K., and Vallier, L. (2012). Inhibition of activin/nodal signalling is necessary for pancreatic differentiation of human pluripotent stem cells. Diabetologia *55*, 3284-3295.

Clevers, H. (2016). Modeling Development and Disease with Organoids. Cell *165*, 1586-1597.

Cogger, K.F., Sinha, A., Sarangi, F., McGaugh, E.C., Saunders, D., Dorrell, C., Mejia-Guerrero, S., Aghazadeh, Y., Rourke, J.L., and Screaton, R.A. (2017). Glycoprotein 2 is a specific cell surface marker of human pancreatic progenitors. Nature Communications *8*, 1-13.

Cohrs, C.M., Chen, C., Jahn, S.R., Stertmann, J., Chmelova, H., Weitz, J., Bahr, A., Klymiuk, N., Steffen, A., Ludwig, B.*, et al.* (2017). Vessel Network Architecture of Adult Human Islets Promotes Distinct Cell-Cell Interactions In Situ and Is Altered After Transplantation. Endocrinology *158*, 1373-1385.

Cohrs, C.M., Chen, C., and Speier, S. (2020). Transplantation of Islets of Langerhans into the Anterior Chamber of the Eye for Longitudinal In Vivo Imaging. Methods Mol Biol *2128*, 149-157.

Collado, M., Gil, J., Efeyan, A., Guerra, C., Schuhmacher, A.J., Barradas, M., Benguría, A., Zaballos, A., Flores, J.M., Barbacid, M.*, et al.* (2005). Senescence in premalignant tumours. Nature *436*, 642-642.

Cox, J., and Mann, M. (2008). MaxQuant enables high peptide identification rates, individualized ppb-range mass accuracies and proteome-wide protein quantification. Nature biotechnology *26*, 1367-1372.

Czodrowski, P., Mallinger, A., Wienke, D., Esdar, C., Pöschke, O., Busch, M., Rohdich, F., Eccles, S.A., Ortiz-Ruiz, M.J., Schneider, R.*, et al.* (2016). Structure-Based Optimization of Potent, Selective, and Orally Bioavailable CDK8 Inhibitors Discovered by High-Throughput Screening. J Med Chem *59*, 9337-9349.

Dantes, Z., Yen, H.-Y., Pfarr, N., Winter, C., Steiger, K., Muckenhuber, A., Hennig, A., Lange, S., Engleitner, T., and Öllinger, R. (2020). Implementing cell-free DNA of pancreatic cancer patient–derived organoids for personalized oncology. JCI insight *5*.

de Lichtenberg, K.H., Seymour, P.A., Jørgensen, M.C., Kim, Y.-H., Grapin-Botton, A., Magnuson, M.A., Nakic, N., Ferrer, J., and Serup, P. (2018). Notch Controls Multiple Pancreatic Cell Fate Regulators Through Direct Hes1-mediated Repression. bioRxiv, 336305.

Dekkers, J.F., Wiegerinck, C.L., de Jonge, H.R., Bronsveld, I., Janssens, H.M., de Winter-de Groot, K.M., Brandsma, A.M., de Jong, N.W., Bijvelds, M.J., Scholte, B.J.*, et al.* (2013). A functional CFTR assay using primary cystic fibrosis intestinal organoids. Nature medicine *19*, 939-945.

Di Micco, R., Fumagalli, M., Cicalese, A., Piccinin, S., Gasparini, P., Luise, C., Schurra, C., Garre, M., Nuciforo, P.G., Bensimon, A*., et al.* (2006). Oncogene-induced senescence is a DNA damage response triggered by DNA hyper-replication. Nature *444*, 638-642.

Ding, Q., Regan, S.N., Xia, Y., Oostrom, L.A., Cowan, C.A., and Musunuru, K. (2013). Enhanced efficiency of human pluripotent stem cell genome editing through replacing TALENs with CRISPRs. Cell stem cell *12*, 393-394.

Dobin, A., Davis, C.A., Schlesinger, F., Drenkow, J., Zaleski, C., Jha, S., Batut, P., Chaisson, M., and Gingeras, T.R. (2013). STAR: ultrafast universal RNA-seq aligner. Bioinformatics *29*, 15-21.

Enge, M., Arda, H.E., Mignardi, M., Beausang, J., Bottino, R., Kim, S.K., and Quake, S.R. (2017). Single-Cell Analysis of Human Pancreas Reveals Transcriptional Signatures of Aging and Somatic Mutation Patterns. Cell *171*, 321-330.e314.

Ferreira, R.M.M., Sancho, R., Messal, H.A., Nye, E., Spencer-Dene, B., Stone, R.K., Stamp, G., Rosewell, I., Quaglia, A., and Behrens, A. (2017). Duct- and Acinar-Derived Pancreatic Ductal Adenocarcinomas Show Distinct Tumor Progression and Marker Expression. Cell Rep *21*, 966-978.

Frejno, M., Chiozzi, R.Z., Wilhelm, M., Koch, H., Zheng, R., Klaeger, S., Ruprecht, B., Meng, C., Kramer, K., and Jarzab, A. (2017). Pharmacoproteomic characterisation of human colon and rectal cancer. Molecular systems biology *13*.

Frishberg, A., Peshes-Yaloz, N., Cohn, O., Rosentul, D., Steuerman, Y., Valadarsky, L., Yankovitz, G., Mandelboim, M., Iraqi, F.A., Amit, I*., et al.* (2019). Cell composition analysis of bulk genomics using single-cell data. Nat Methods *16*, 327-332.

Fryer, C.J., White, J.B., and Jones, K.A. (2004). Mastermind recruits CycC:CDK8 to phosphorylate the Notch ICD and coordinate activation with turnover. Mol Cell *16*, 509-520.

Furukawa, T., Kloppel, G., Volkan Adsay, N., Albores-Saavedra, J., Fukushima, N., Horii, A., Hruban, R.H., Kato, Y., Klimstra, D.S., Longnecker, D.S*., et al.* (2005). Classification of types of intraductal papillary-mucinous neoplasm of the pancreas: a consensus study. Virchows Arch *447*, 794-799.

Gaujoux, S., Salenave, S., Ronot, M., Rangheard, A.S., Cros, J., Belghiti, J., Sauvanet, A., Ruszniewski, P., and Chanson, P. (2014). Hepatobiliary and Pancreatic neoplasms in patients with McCune-Albright syndrome. J Clin Endocrinol Metab *99*, E97-101.

Georgakopoulos, N., Prior, N., Angres, B., Mastrogiovanni, G., Cagan, A., Harrison, D., Hindley, C.J., Arnes-Benito, R., Liau, S.S., Curd, A*., et al.* (2020). Long-term expansion, genomic stability and in vivo safety of adult human pancreas organoids. BMC Dev Biol *20*, 4.

Gerrard, D.T., Berry, A.A., Jennings, R.E., Piper Hanley, K., Bobola, N., and Hanley, N.A. (2016). An integrative transcriptomic atlas of organogenesis in human embryos. Elife *5*.

Gliwicz, D., Jankowska, I., Wierzbicka, A., Miskiewicz-Chotnicka, A., Lisowska, A., and Walkowiak, J. (2016). Exocrine pancreatic function in children with Alagille syndrome. Sci Rep *6*, 35229.

Gloeckner, C.J., Boldt, K., Schumacher, A., and Ueffing, M. (2009). Tandem affinity purification of protein complexes from mammalian cells by the Strep/FLAG (SF)-TAP tag. In Proteomics (Springer), pp. 359-372.

Golson, M.L., Loomes, K.M., Oakey, R., and Kaestner, K.H. (2009). Ductal malformation and pancreatitis in mice caused by conditional Jag1 deletion. Gastroenterology *136*, 1761-1771 e1761.

Gout, J., Perkhofer, L., Morawe, M., Arnold, F., Ihle, M., Biber, S., Lange, S., Roger, E., Kraus, J.M., Stifter, K*., et al.* (2020). Synergistic targeting and resistance to PARP inhibition in DNA damage repair-deficient pancreatic cancer. Gut.

Grigore, A.D., Jolly, M.K., Jia, D., Farach-Carson, M.C., and Levine, H. (2016). Tumor Budding: The Name is EMT. Partial EMT. Journal of clinical medicine *5*.

Haeussler, M., Schonig, K., Eckert, H., Eschstruth, A., Mianne, J., Renaud, J.B., Schneider-Maunoury, S., Shkumatava, A., Teboul, L., Kent, J*., et al.* (2016). Evaluation of off-target and on-target scoring algorithms and integration into the guide RNA selection tool CRISPOR. Genome Biol *17*, 148.

Heng, L. (2013). Aligning sequence reads, clone sequences and assembly contigs with BWA-MEM (arXiv).

Hogrebe, N.J., Augsornworawat, P., Maxwell, K.G., Velazco-Cruz, L., and Millman, J.R. (2020). Targeting the cytoskeleton to direct pancreatic differentiation of human pluripotent stem cells. Nat Biotechnol.

Hohwieler, M., Illing, A., Hermann, P.C., Mayer, T., Stockmann, M., Perkhofer, L., Eiseler, T., Antony, J.S., Muller, M., Renz, S*., et al.* (2017a). Human pluripotent stem cell-derived acinar/ductal organoids generate human pancreas upon orthotopic transplantation and allow disease modelling. Gut *66*, 473-486.

Hohwieler, M., Muller, M., Frappart, P.O., and Heller, S. (2019). Pancreatic Progenitors and Organoids as a Prerequisite to Model Pancreatic Diseases and Cancer. Stem Cells Int *2019*, 9301382.

Hohwieler, M., Perkhofer, L., Liebau, S., Seufferlein, T., Muller, M., Illing, A., and Kleger, A. (2017b). Stem cell-derived organoids to model gastrointestinal facets of cystic fibrosis. United European Gastroenterol J *5*, 609-624.

Hua, H., Zhang, Y.Q., Dabernat, S., Kritzik, M., Dietz, D., Sterling, L., and Sarvetnick, N. (2006). BMP4 regulates pancreatic progenitor cell expansion through Id2. J Biol Chem *281*, 13574-13580.

Huang, L., Holtzinger, A., Jagan, I., BeGora, M., Lohse, I., Ngai, N., Nostro, C., Wang, R., Muthuswamy, L.B., Crawford, H.C*., et al.* (2015). Ductal pancreatic cancer modeling and drug screening using human pluripotent stem cell- and patient-derived tumor organoids. Nature medicine *21*, 1364-1371.

Huch, M., Gehart, H., van Boxtel, R., Hamer, K., Blokzijl, F., Verstegen, M.M., Ellis, E., van Wenum, M., Fuchs, S.A., de Ligt, J*., et al.* (2015). Long-term culture of genome-stable bipotent stem cells from adult human liver. Cell *160*, 299-312.

Ideno, N., Yamaguchi, H., Ghosh, B., Gupta, S., Okumura, T., Steffen, D.J., Fisher, C.G., Wood, L.D., Singhi, A.D., Nakamura, M*., et al.* (2018). GNAS(R201C) Induces Pancreatic Cystic Neoplasms in Mice That Express Activated KRAS by Inhibiting YAP1 Signaling. Gastroenterology.

Illing, A., Stockmann, M., Swamy Telugu, N., Linta, L., Russell, R., Muller, M., Seufferlein, T., Liebau, S., and Kleger, A. (2013). Definitive Endoderm Formation from Plucked Human Hair-Derived Induced Pluripotent Stem Cells and SK Channel Regulation. Stem Cells International *2013*, 360573.

Jennings, R.E., Berry, A.A., Kirkwood-Wilson, R., Roberts, N.A., Hearn, T., Salisbury, R.J., Blaylock, J., Piper Hanley, K., and Hanley, N.A. (2013). Development of the human pancreas from foregut to endocrine commitment. Diabetes *62*, 3514-3522.

Johnson, W.E., Li, C., and Rabinovic, A. (2007). Adjusting batch effects in microarray expression data using empirical Bayes methods. Biostatistics *8*, 118-127.

Kang, J.H., Hwang, S.M., and Chung, I.Y. (2015). S100A8, S100A9 and S100A12 activate airway epithelial cells to produce MUC5AC via extracellular signal-regulated kinase and nuclear factor-kappaB pathways. Immunology *144*, 79-90.

Kesavan, G., Sand, F.W., Greiner, T.U., Johansson, J.K., Kobberup, S., Wu, X., Brakebusch, C., and Semb, H. (2009). Cdc42-mediated tubulogenesis controls cell specification. Cell *139*, 791-801.

Kim, S.I., Oceguera-Yanez, F., Sakurai, C., Nakagawa, M., Yamanaka, S., and Woltjen, K. (2016). Inducible Transgene Expression in Human iPS Cells Using Versatile All-in-One piggyBac Transposons. Methods Mol Biol *1357*, 111-131.

Klausen, P., Kovacevic, B., Toxvaerd, A., Kalaitzakis, E., Karstensen, J.G., Rift, C.V., Hansen, C.P., Storkholm, J., Vilmann, P., and Hasselby, J.P. (2019). Subtyping of intraductal papillary mucinous neoplasms - pitfalls of MUC1 immunohistochemistry. Apmis *127*, 27-32.

Koike, H., Iwasawa, K., Ouchi, R., Maezawa, M., Giesbrecht, K., Saiki, N., Ferguson, A., Kimura, M., Thompson, W.L., Wells, J.M*., et al.* (2019). Modelling human hepato-biliary-pancreatic organogenesis from the foregut-midgut boundary. Nature *574*, 112-116.

Kopp, J.L., Dubois, C.L., Schaeffer, D.F., Samani, A., Taghizadeh, F., Cowan, R.W., Rhim, A.D., Stiles, B.L., Valasek, M., and Sander, M. (2018). Loss of Pten and Activation of Kras Synergistically Induce Formation of Intraductal Papillary Mucinous Neoplasia From Pancreatic Ductal Cells in Mice. Gastroenterology *154*, 1509-1523 e1505.

Kopp, J.L., von Figura, G., Mayes, E., Liu, F.F., Dubois, C.L., Morris, J.P.t., Pan, F.C., Akiyama, H., Wright, C.V., Jensen, K*., et al.* (2012). Identification of Sox9-dependent acinar-to-ductal reprogramming as the principal mechanism for initiation of pancreatic ductal adenocarcinoma. Cancer Cell *22*, 737-750.

Korytnikov, R., and Nostro, M.C. (2016). Generation of polyhormonal and multipotent pancreatic progenitor lineages from human pluripotent stem cells. Methods *101*, 56-64.

Krentz, N.A.J., Lee, M.Y.Y., Xu, E.E., Sproul, S.L.J., Maslova, A., Sasaki, S., and Lynn, F.C. (2018). Single-Cell Transcriptome Profiling of Mouse and hESC-Derived Pancreatic Progenitors. Stem Cell Reports *11*, 1551-1564.

Kuilman, T. (2020). CopywriteR: Copy number information from targeted sequencing using off-target reads (Bioconductor from within R).

Kuilman, T., Michaloglou, C., Vredeveld, L.C., Douma, S., van Doorn, R., Desmet, C.J., Aarden, L.A., Mooi, W.J., and Peeper, D.S. (2008). Oncogene-induced senescence relayed by an interleukin-dependent inflammatory network. Cell *133*, 1019-1031.

Kuleshov, M.V., Jones, M.R., Rouillard, A.D., Fernandez, N.F., Duan, Q., Wang, Z., Koplev, S., Jenkins, S.L., Jagodnik, K.M., and Lachmann, A. (2016). Enrichr: a comprehensive gene set enrichment analysis web server 2016 update. Nucleic acids research *44*, W90-W97.

Lee, A.Y.L., Dubois, C.L., Sarai, K., Zarei, S., Schaeffer, D.F., Sander, M., and Kopp, J.L. (2018). Cell of origin affects tumour development and phenotype in pancreatic ductal adenocarcinoma. Gut.

Lee, S., and Schmitt, C.A. (2019). The dynamic nature of senescence in cancer. Nature cell biology *21*, 94-101.

Leek, J.T., Johnson, W.E., Parker, H.S., Jaffe, A.E., and Storey, J.D. (2012). The sva package for removing batch effects and other unwanted variation in high-throughput experiments. Bioinformatics *28*, 882-883.

Lesina, M., Wormann, S.M., Morton, J., Diakopoulos, K.N., Korneeva, O., Wimmer, M., Einwachter, H., Sperveslage, J., Demir, I.E., Kehl, T*., et al.* (2016). RelA regulates CXCL1/CXCR2-dependent oncogene-induced senescence in murine Kras-driven pancreatic carcinogenesis. The Journal of clinical investigation *126*, 2919-2932.

Levine, J.H., Simonds, E.F., Bendall, S.C., Davis, K.L., Amir el, A.D., Tadmor, M.D., Litvin, O., Fienberg, H.G., Jager, A., Zunder, E.R*., et al.* (2015). Data-Driven Phenotypic Dissection of AML Reveals Progenitor-like Cells that Correlate with Prognosis. Cell *162*, 184-197.

Li, Y., Deng, S., Peng, J., Wang, X., Essandoh, K., Mu, X., Peng, T., Meng, Z.X., and Fan, G.C. (2019). MicroRNA-223 is essential for maintaining functional beta-cell mass during diabetes through inhibiting both FOXO1 and SOX6 pathways. J Biol Chem *294*, 10438-10448.

Liao, Y., Smyth, G.K., and Shi, W. (2019). The R package Rsubread is easier, faster, cheaper and better for alignment and quantification of RNA sequencing reads. Nucleic Acids Research *47*, e47-e47.

Lin, A.W., Barradas, M., Stone, J.C., van Aelst, L., Serrano, M., and Lowe, S.W. (1998). Premature senescence involving p53 and p16 is activated in response to constitutive MEK/MAPK mitogenic signaling. Genes & development *12*, 3008-3019.

Linta, L., Stockmann, M., Kleinhans, K.N., Bockers, A., Storch, A., Zaehres, H., Lin, Q., Barbi, G., Bockers, T.M., Kleger, A.*, et al.* (2012). Rat embryonic fibroblasts improve reprogramming of human keratinocytes into induced pluripotent stem cells. Stem cells and development *21*, 965-976.

Love, M.I., Huber, W., and Anders, S. (2014). Moderated estimation of fold change and dispersion for RNA-seq data with DESeq2. Genome biology *15*, 550.

Lun, A.T., McCarthy, D.J., and Marioni, J.C. (2016). A step-by-step workflow for low-level analysis of single-cell RNA-seq data with Bioconductor. F1000Res *5*, 2122.

Ma, H., Wert, K.J., Shvartsman, D., Melton, D.A., and Jaenisch, R. (2018). Establishment of human pluripotent stem cell-derived pancreatic β-like cells in the mouse pancreas. Proc Natl Acad Sci U S A *115*, 3924-3929.

Macosko, E.Z., Basu, A., Satija, R., Nemesh, J., Shekhar, K., Goldman, M., Tirosh, I., Bialas, A.R., Kamitaki, N., and Martersteck, E.M. (2015). Highly parallel genome-wide expression profiling of individual cells using nanoliter droplets. Cell *161*, 1202-1214.

Maléth, J., Balázs, A., Pallagi, P., Balla, Z., Kui, B., Katona, M., Judák, L., Németh, I., Kemény, L.V., Rakonczay, Z., Jr.*, et al.* (2015). Alcohol disrupts levels and function of the cystic fibrosis transmembrane conductance regulator to promote development of pancreatitis. Gastroenterology *148*, 427-439.e416.

Mali, P., Yang, L., Esvelt, K.M., Aach, J., Guell, M., DiCarlo, J.E., Norville, J.E., and Church, G.M. (2013). RNA-guided human genome engineering via Cas9. Science *339*, 823-826.

McInnes, L., Healy, J., and Melville, J. (2018). Umap: Uniform manifold approximation and projection for dimension reduction. arXiv preprint arXiv:180203426.

Messal, H.A., Alt, S., Ferreira, R.M.M., Gribben, C., Wang, V.M., Cotoi, C.G., Salbreux, G., and Behrens, A. (2019). Tissue curvature and apicobasal mechanical tension imbalance instruct cancer morphogenesis. Nature *566*, 126-130.

Moffitt, R.A., Marayati, R., Flate, E.L., Volmar, K.E., Loeza, S.G., Hoadley, K.A., Rashid, N.U., Williams, L.A., Eaton, S.C., Chung, A.H.*, et al.* (2015). Virtual microdissection identifies distinct tumor- and stroma-specific subtypes of pancreatic ductal adenocarcinoma. Nat Genet *47*, 1168-1178.

Molnár, R., Madácsy, T., Varga, Á., Németh, M., Katona, X., Görög, M., Molnár, B., Fanczal, J., Rakonczay, Z., and Hegyi, P. (2020). Mouse pancreatic ductal organoid culture as a relevant model to study exocrine pancreatic ion secretion. Laboratory Investigation *100*, 84-97.

Moreira, L., Bakir, B., Chatterji, P., Dantes, Z., Reichert, M., and Rustgi, A.K. (2018). Pancreas 3D Organoids: Current and Future Aspects as a Research Platform for Personalized Medicine in Pancreatic Cancer. Cellular and molecular gastroenterology and hepatology *5*, 289-298.

Morton, J.P., Timpson, P., Karim, S.A., Ridgway, R.A., Athineos, D., Doyle, B., Jamieson, N.B., Oien, K.A., Lowy, A.M., Brunton, V.G.*, et al.* (2010). Mutant p53 drives metastasis and overcomes growth arrest/senescence in pancreatic cancer. Proc Natl Acad Sci U S A *107*, 246-251.

Mueller, S., Engleitner, T., Maresch, R., Zukowska, M., Lange, S., Kaltenbacher, T., Konukiewitz, B., Ollinger, R., Zwiebel, M., Strong, A.*, et al.* (2018). Evolutionary routes and KRAS dosage define pancreatic cancer phenotypes. Nature *554*, 62-68.

Nostro, M.C., Sarangi, F., Yang, C., Holland, A., Elefanty, A.G., Stanley, E.G., Greiner, D.L., and Keller, G. (2015). Efficient generation of NKX6-1+ pancreatic progenitors from multiple human pluripotent stem cell lines. Stem Cell Reports *4*, 591-604.

Notta, F., Chan-Seng-Yue, M., Lemire, M., Li, Y., Wilson, G.W., Connor, A.A., Denroche, R.E., Liang, S.B., Brown, A.M., Kim, J.C*., et al.* (2016). A renewed model of pancreatic cancer evolution based on genomic rearrangement patterns. Nature *538*, 378-382.

O'Hayre, M., Vazquez-Prado, J., Kufareva, I., Stawiski, E.W., Handel, T.M., Seshagiri, S., and Gutkind, J.S. (2013). The emerging mutational landscape of G proteins and G-protein-coupled receptors in cancer. Nature reviews Cancer *13*, 412-424.

Ohashi, S., Natsuizaka, M., Wong, G.S., Michaylira, C.Z., Grugan, K.D., Stairs, D.B., Kalabis, J., Vega, M.E., Kalman, R.A., Nakagawa, M*., et al.* (2010). Epidermal growth factor receptor and mutant p53 expand an esophageal cellular subpopulation capable of epithelial-to-mesenchymal transition through ZEB transcription factors. Cancer Res *70*, 4174-4184.

Parekh, S., Ziegenhain, C., Vieth, B., Enard, W., and Hellmann, I. (2016). The impact of amplification on differential expression analyses by RNA-seq. Scientific reports *6*, 25533.

Parvanescu, A., Cros, J., Ronot, M., Hentic, O., Grybek, V., Couvelard, A., Levy, P., Chanson, P., Ruszniewski, P., Sauvanet, A*., et al.* (2014). Lessons from McCune-Albright syndrome-associated intraductal papillary mucinous neoplasms: : GNAS-activating mutations in pancreatic carcinogenesis. JAMA Surg *149*, 858-862.

Patra, K.C., Bardeesy, N., and Mizukami, Y. (2017). Diversity of Precursor Lesions For Pancreatic Cancer: The Genetics and Biology of Intraductal Papillary Mucinous Neoplasm. Clinical and translational gastroenterology *8*, e86.

Patra, K.C., Kato, Y., Mizukami, Y., Widholz, S., Boukhali, M., Revenco, I., Grossman, E.A., Ji, F., Sadreyev, R.I., Liss, A.S*., et al.* (2018). Mutant GNAS drives pancreatic tumourigenesis by inducing PKA-mediated SIK suppression and reprogramming lipid metabolism. Nature cell biology *20*, 811-822.

Perez-Riverol, Y., Csordas, A., Bai, J., Bernal-Llinares, M., Hewapathirana, S., Kundu, D.J., Inuganti, A., Griss, J., Mayer, G., Eisenacher, M*., et al.* (2019). The PRIDE database and related tools and resources in 2019: improving support for quantification data. Nucleic Acids Res *47*, D442-d450.

Perkhofer, L., Schmitt, A., Romero Carrasco, M.C., Ihle, M., Hampp, S., Ruess, D.A., Hessmann, E., Russell, R., Lechel, A., Azoitei, N*., et al.* (2017). ATM Deficiency Generating Genomic Instability Sensitizes Pancreatic Ductal Adenocarcinoma Cells to Therapy-Induced DNA Damage. Cancer research *77*, 5576-5590.

Poplin, R., Ruano-Rubio, V., DePristo, M.A., Fennell, T.J., Carneiro, M.O., Van der Auwera, G.A., Kling, D.E., Gauthier, L.D., Levy-Moonshine, A., Roazen, D*., et al.* (2018). Scaling accurate genetic variant discovery to tens of thousands of samples. bioRxiv, 201178.

Puleo, F., Nicolle, R., Blum, Y., Cros, J., Marisa, L., Demetter, P., Quertinmont, E., Svrcek, M., Elarouci, N., Iovanna, J*., et al.* (2018). Stratification of Pancreatic Ductal Adenocarcinomas Based on Tumor and Microenvironment Features. Gastroenterology *155*, 1999-2013.e1993.

Qadir, M.M.F., Álvarez-Cubela, S., Klein, D., van Dijk, J., Muñiz-Anquela, R., Moreno-Hernández, Y.B., Lanzoni, G., Sadiq, S., Navarro-Rubio, B., García, M.T*., et al.* (2020). Single-cell resolution analysis of the human pancreatic ductal progenitor cell niche. Proc Natl Acad Sci U S A *117*, 10876-10887.

Qi, H., Yao, L., and Liu, Q. (2019). MicroRNA-96 regulates pancreatic beta cell function under the pathological condition of diabetes mellitus through targeting Foxo1 and Sox6. Biochem Biophys Res Commun *519*, 294-301.

Rahib, L., Smith, B.D., Aizenberg, R., Rosenzweig, A.B., Fleshman, J.M., and Matrisian, L.M. (2014). Projecting cancer incidence and deaths to 2030: the unexpected burden of thyroid, liver, and pancreas cancers in the United States. Cancer Res *74*, 2913-2921.

Rao, J., Pfeiffer, M.J., Frank, S., Adachi, K., Piccini, I., Quaranta, R., Araúzo-Bravo, M., Schwarz, J., Schade, D., and Leidel, S. (2016). Stepwise clearance of repressive roadblocks drives cardiac induction in human ESCs. Cell stem cell *18*, 341-353.

Ray, K.C., Bell, K.M., Yan, J., Gu, G., Chung, C.H., Washington, M.K., and Means, A.L. (2011). Epithelial tissues have varying degrees of susceptibility to Kras(G12D)-initiated tumorigenesis in a mouse model. PLoS One *6*, e16786.

Reichert, M., Blume, K., Kleger, A., Hartmann, D., and von Figura, G. (2016). Developmental Pathways Direct Pancreatic Cancer Initiation from Its Cellular Origin. Stem Cells Int *2016*, 9298535.

Renz, B.W., Takahashi, R., Tanaka, T., Macchini, M., Hayakawa, Y., Dantes, Z., Maurer, H.C., Chen, X., Jiang, Z., and Westphalen, C.B. (2018a). β2 adrenergic-neurotrophin feedforward loop promotes pancreatic cancer. Cancer cell *33*, 75-90. e77.

Renz, B.W., Tanaka, T., Sunagawa, M., Takahashi, R., Jiang, Z., Macchini, M., Dantes, Z., Valenti, G., White, R.A., and Middelhoff, M.A. (2018b). Cholinergic signaling via muscarinic receptors directly and indirectly suppresses pancreatic tumorigenesis and cancer stemness. Cancer discovery *8*, 1458-1473.

Rezanejad, H., Ouziel-Yahalom, L., Keyzer, C.A., Sullivan, B.A., Hollister-Lock, J., Li, W.C., Guo, L., Deng, S., Lei, J., Markmann, J.*, et al.* (2018). Heterogeneity of SOX9 and HNF1beta in Pancreatic Ducts Is Dynamic. Stem Cell Reports *10*, 725-738.

Rezania, A., Bruin, J.E., Riedel, M.J., Mojibian, M., Asadi, A., Xu, J., Gauvin, R., Narayan, K., Karanu, F., O'Neil, J.J.*, et al.* (2012). Maturation of human embryonic stem cell-derived pancreatic progenitors into functional islets capable of treating pre-existing diabetes in mice. Diabetes *61*, 2016-2029.

Rhodes, J.A., Criscimanna, A., and Esni, F. (2012). Induction of mouse pancreatic ductal differentiation, an in vitro assay. In Vitro Cell Dev Biol Anim *48*, 641-649.

Ritchie, M.E., Phipson, B., Wu, D., Hu, Y., Law, C.W., Shi, W., and Smyth, G.K. (2015). limma powers differential expression analyses for RNA-sequencing and microarray studies. Nucleic Acids Res *43*, e47.

Roberts, N.J., Norris, A.L., Petersen, G.M., Bondy, M.L., Brand, R., Gallinger, S., Kurtz, R.C., Olson, S.H., Rustgi, A.K., Schwartz, A.G.*, et al.* (2016). Whole Genome Sequencing Defines the Genetic Heterogeneity of Familial Pancreatic Cancer. Cancer Discov *6*, 166-175.

Robinson, C., Estrada, A., Zaheer, A., Singh, V.K., Wolfgang, C.L., Goggins, M.G., Hruban, R.H., Wood, L.D., Noe, M., Montgomery, E.A.*, et al.* (2018). Clinical and Radiographic Gastrointestinal Abnormalities in McCune-Albright Syndrome. J Clin Endocrinol Metab *103*, 4293-4303.

Robinson, J.T., Thorvaldsdóttir, H., Winckler, W., Guttman, M., Lander, E.S., Getz, G., and Mesirov, J.P. (2011). Integrative genomics viewer. In Nat Biotechnol, pp. 24-26.

Rosenbaum, D.M., Rasmussen, S.G., and Kobilka, B.K. (2009). The structure and function of G-protein-coupled receptors. Nature *459*, 356-363.

Rovira, M., Delaspre, F., Massumi, M., Serra, S.A., Valverde, M.A., Lloreta, J., Dufresne, M., Payré, B., Konieczny, S.F., Savatier, P.*, et al.* (2008). Murine embryonic stem cell-derived pancreatic acinar cells recapitulate features of early pancreatic differentiation. Gastroenterology *135*, 1301-1310, 1310.e1301-1305.

Rowe, R.G., and Daley, G.Q. (2019). Induced pluripotent stem cells in disease modelling and drug discovery. Nat Rev Genet *20*, 377-388.

Rubio-Viqueira, B., Jimeno, A., Cusatis, G., Zhang, X., Iacobuzio-Donahue, C., Karikari, C., Shi, C., Danenberg, K., Danenberg, P.V., Kuramochi, H.*, et al.* (2006). An in vivo platform for translational drug development in pancreatic cancer. Clin Cancer Res *12*, 4652-4661.

Ruess, D.A., Heynen, G.J., Ciecielski, K.J., Ai, J., Berninger, A., Kabacaoglu, D., Görgülü, K., Dantes, Z., Wörmann, S.M., and Diakopoulos, K.N. (2018). Mutant KRAS-driven cancers depend on PTPN11/SHP2 phosphatase. Nature medicine *24*, 954-960.

Salinas-Souza, C., De Andrea, C., Bihl, M., Kovac, M., Pillay, N., Forshew, T., Gutteridge, A., Ye, H., Amary, M.F., Tirabosco, R.*, et al.* (2015). GNAS mutations are not detected in parosteal and low-grade central osteosarcomas. Mod Pathol *28*, 1336-1342.

Sassone-Corsi, P. (2012). The cyclic AMP pathway. Cold Spring Harbor perspectives in biology *4*.

Sato, T., Vries, R.G., Snippert, H.J., van de Wetering, M., Barker, N., Stange, D.E., van Es, J.H., Abo, A., Kujala, P., Peters, P.J.*, et al.* (2009). Single Lgr5 stem cells build crypt-villus structures in vitro without a mesenchymal niche. Nature *459*, 262-265.

Schaffer, A.E., Freude, K.K., Nelson, S.B., and Sander, M. (2010). Nkx6 transcription factors and Ptf1a function as antagonistic lineage determinants in multipotent pancreatic progenitors. Developmental cell *18*, 1022-1029.

Schindelin, J., Arganda-Carreras, I., Frise, E., Kaynig, V., Longair, M., Pietzsch, T., Preibisch, S., Rueden, C., Saalfeld, S., Schmid, B.*, et al.* (2012). Fiji: an open-source platform for biological-image analysis. Nat Methods *9*, 676-682.

Seino, T., Kawasaki, S., Shimokawa, M., Tamagawa, H., Toshimitsu, K., Fujii, M., Ohta, Y., Matano, M., Nanki, K., Kawasaki, K.*, et al.* (2018). Human Pancreatic Tumor Organoids Reveal Loss of Stem Cell Niche Factor Dependence during Disease Progression. Cell stem cell *22*, 454-467 e456.

Serrano, M., Lin, A.W., McCurrach, M.E., Beach, D., and Lowe, S.W. (1997). Oncogenic ras provokes premature cell senescence associated with accumulation of p53 and p16INK4a. Cell *88*, 593-602.

Shain, A.H., Giacomini, C.P., Matsukuma, K., Karikari, C.A., Bashyam, M.D., Hidalgo, M., Maitra, A., and Pollack, J.R. (2012). Convergent structural alterations define SWItch/Sucrose NonFermentable (SWI/SNF) chromatin remodeler as a central tumor suppressive complex in pancreatic cancer. Proc Natl Acad Sci U S A *109*, E252-259.

Shih, H.P., Wang, A., and Sander, M. (2013). Pancreas organogenesis: from lineage determination to morphogenesis. Annual review of cell and developmental biology *29*, 81-105.

Smit, M.A., and Peeper, D.S. (2008). Deregulating EMT and senescence: double impact by a single twist. Cancer Cell *14*, 5-7.

Song, J. (2007). EMT or apoptosis: a decision for TGF-beta. Cell Res *17*, 289-290.

Song, J., and Shi, W. (2018). The concomitant apoptosis and EMT underlie the fundamental functions of TGF-β. Acta Biochim Biophys Sin (Shanghai) *50*, 91-97.

Springer, S., Wang, Y., Dal Molin, M., Masica, D.L., Jiao, Y., Kinde, I., Blackford, A., Raman, S.P., Wolfgang, C.L., Tomita, T.*, et al.* (2015). A combination of molecular markers and clinical features improve the classification of pancreatic cysts. Gastroenterology *149*, 1501-1510.

Subramanian, A., Tamayo, P., Mootha, V.K., Mukherjee, S., Ebert, B.L., Gillette, M.A., Paulovich, A., Pomeroy, S.L., Golub, T.R., and Lander, E.S. (2005). Gene set enrichment analysis: a knowledge-based approach for interpreting genome-wide expression profiles. Proceedings of the National Academy of Sciences *102*, 15545-15550.

Takebe, T., Sekine, K., Kimura, M., Yoshizawa, E., Ayano, S., Koido, M., Funayama, S., Nakanishi, N., Hisai, T., Kobayashi, T.*, et al.* (2017). Massive and Reproducible Production of Liver Buds Entirely from Human Pluripotent Stem Cells. Cell Rep *21*, 2661-2670.

Takeuchi, S., Takahashi, A., Motoi, N., Yoshimoto, S., Tajima, T., Yamakoshi, K., Hirao, A., Yanagi, S., Fukami, K., Ishikawa, Y.*, et al.* (2010). Intrinsic cooperation between p16INK4a and p21Waf1/Cip1 in the onset of cellular senescence and tumor suppression in vivo. Cancer Res *70*, 9381-9390.

Taki, K., Ohmuraya, M., Tanji, E., Komatsu, H., Hashimoto, D., Semba, K., Araki, K., Kawaguchi, Y., Baba, H., and Furukawa, T. (2016). GNAS(R201H) and Kras(G12D) cooperate to promote murine pancreatic tumorigenesis recapitulating human intraductal papillary mucinous neoplasm. Oncogene *35*, 2407-2412.

Tan, M.C., Basturk, O., Brannon, A.R., Bhanot, U., Scott, S.N., Bouvier, N., LaFemina, J., Jarnagin, W.R., Berger, M.F., Klimstra, D.*, et al.* (2015). GNAS and KRAS Mutations Define Separate Progression Pathways in Intraductal Papillary Mucinous Neoplasm-Associated Carcinoma. Journal of the American College of Surgeons *220*, 845-854.e841.

Tarasov, A., Vilella, A.J., Cuppen, E., Nijman, I.J., and Prins, P. (2015). Sambamba: fast processing of NGS alignment formats. Bioinformatics *31*, 2032-2034.

Tiriac, H., Bucobo, J.C., Tzimas, D., Grewel, S., Lacomb, J.F., Rowehl, L.M., Nagula, S., Wu, M., Kim, J., Sasson, A.*, et al.* (2018). Successful creation of pancreatic cancer organoids by means of EUS-guided fine-needle biopsy sampling for personalized cancer treatment. Gastrointest Endosc *87*, 1474-1480.

Topno, N.S., Kannan, M., and Krishna, R. (2018). Mechanistic insights into the activity of Ptf1-p48 (pancreas transcription factor 1a): probing the interactions levels of Ptf1-p48 with E2A-E47 (transcription factor E2-alpha) and ID3 (inhibitor of DNA binding 3). J Biomol Struct Dyn *36*, 1834-1852.

Traag, V. (2015). louvain-igraph: v0.5.3 (Version v0.5.3). Zenodo. (Zenodo).

Tu, Q., Hao, J., Zhou, X., Yan, L., Dai, H., Sun, B., Yang, D., An, S., Lv, L., Jiao, B.*, et al.* (2018). CDKN2B deletion is essential for pancreatic cancer development instead of unmeaningful co-deletion due to juxtaposition to CDKN2A. Oncogene *37*, 128-138.

Tulpule, A., Kelley, J.M., Lensch, M.W., McPherson, J., Park, I.H., Hartung, O., Nakamura, T., Schlaeger, T.M., Shimamura, A., and Daley, G.Q. (2013). Pluripotent stem cell models of Shwachman-Diamond syndrome reveal a common mechanism for pancreatic and hematopoietic dysfunction. Cell stem cell *12*, 727-736.

Villani, V., Thornton, M.E., Zook, H.N., Crook, C.J., Grubbs, B.H., Orlando, G., De Filippo, R., Ku, H.T., and Perin, L. (2019). SOX9+/PTF1A+ Cells Define the Tip Progenitor Cells of the Human Fetal Pancreas of the Second Trimester. Stem Cells Transl Med *8*, 1249-1264.

Villasenor, A., Chong, D.C., Henkemeyer, M., and Cleaver, O. (2010). Epithelial dynamics of pancreatic branching morphogenesis. Development *137*, 4295-4305.

Warlich, E., Kuehle, J., Cantz, T., Brugman, M.H., Maetzig, T., Galla, M., Filipczyk, A.A., Halle, S., Klump, H., and Schöler, H.R. (2011). Lentiviral vector design and imaging approaches to visualize the early stages of cellular reprogramming. Molecular Therapy *19*, 782-789.

Wilschanski, M., and Novak, I. (2013). The cystic fibrosis of exocrine pancreas. Cold Spring Harb Perspect Med *3*, a009746.

Wolf, F.A., Angerer, P., Ramirez, F., Virshup, I., Rybakov, S., Eraslan, G., White, T., Luecken, M., Cittaro, D., Callies, T.*, et al.* (2020). scanpy.tl.rank_genes_groups.

Wolf, F.A., Angerer, P., and Theis, F.J. (2018). SCANPY: large-scale single-cell gene expression data analysis. Genome Biol *19*, 15.

Wood, L.D., Noë, M., Hackeng, W., Brosens, L.A., Bhaijee, F., Debeljak, M., Yu, J., Suenaga, M., Singhi, A.D., and Zaheer, A. (2017). Patients with McCune-Albright syndrome have a broad spectrum of abnormalities in the gastrointestinal tract and pancreas. Virchows Archiv *470*, 391-400.

Wu, F., Wu, D., Ren, Y., Huang, Y., Feng, B., Zhao, N., Zhang, T., Chen, X., Chen, S., and Xu, A. (2019). Generation of hepatobiliary organoids from human induced pluripotent stem cells. J Hepatol *70*, 1145-1158.

Wu, J., Matthaei, H., Maitra, A., Dal Molin, M., Wood, L.D., Eshleman, J.R., Goggins, M., Canto, M.I., Schulick, R.D., Edil, B.H.*, et al.* (2011). Recurrent GNAS mutations define an unexpected pathway for pancreatic cyst development. Science translational medicine *3*, 92ra66.

Xiang, B., and Muthuswamy, S.K. (2006). Using Three-Dimensional Acinar Structures for Molecular and Cell Biological Assays. Methods in enzymology *406*, 692-701.

Xiao, W., Hong, H., Awadallah, A., Zhou, L., and Xin, W. (2014). Utilization of CDX2 expression in diagnosing pancreatic ductal adenocarcinoma and predicting prognosis. PLoS One *9*, e86853.

Xie, R., Everett, L.J., Lim, H.W., Patel, N.A., Schug, J., Kroon, E., Kelly, O.G., Wang, A., D'Amour, K.A., Robins, A.J., *et al.* (2013). Dynamic chromatin remodeling mediated by polycomb proteins orchestrates pancreatic differentiation of human embryonic stem cells. Cell stem cell *12*, 224-237.

Xiong, J., Zhao, W.Q., Huang, G.H., Yao, L.H., Dong, H.M., Yu, C.H., Zhao, H.J., and Cai, S.X. (2017). [Receptor for advanced glycation end products upregulates MUC5AC expression and promotes mucus overproduction in mice with toluene diisocyanate-induced asthma]. Nan Fang Yi Ke Da Xue Xue Bao *37*, 1301-1307.

Yonezawa, S., Higashi, M., Yamada, N., and Goto, M. (2008). Precursor lesions of pancreatic cancer. Gut Liver *2*, 137-154.

Zecha, J., Satpathy, S., Kanashova, T., Avanessian, S.C., Kane, M.H., Clauser, K.R., Mertins, P., Carr, S.A., and Kuster, B. (2019). TMT Labeling for the Masses: A Robust and Cost-efficient, In-solution Labeling Approach. Mol Cell Proteomics *18*, 1468-1478.

Zeman, M.K., and Cimprich, K.A. (2014). Causes and consequences of replication stress. Nature cell biology *16*, 2-9.

Zhou, Q., Law, A.C., Rajagopal, J., Anderson, W.J., Gray, P.A., and Melton, D.A. (2007). A multipotent progenitor domain guides pancreatic organogenesis. Dev Cell *13*, 103-114.